



Gut mucosa alterations and loss of segmented filamentous bacteria in type 1 diabetes are associated with inflammation rather than hyperglycaemia

Matthieu Rouland, Lucie Beaudoin, Ophélie Rouxel, Léo Bertrand, Lucie Cagninacci, Azadeh Saffarian, Thierry Pedron, Dalale Gueddouri, Sandra Guilmeau, Anne-Françoise Burnol, et al.

► To cite this version:

Matthieu Rouland, Lucie Beaudoin, Ophélie Rouxel, Léo Bertrand, Lucie Cagninacci, et al.. Gut mucosa alterations and loss of segmented filamentous bacteria in type 1 diabetes are associated with inflammation rather than hyperglycaemia. *Gut*, 2022, 71 (2), pp.296-308. 10.1136/gutjnl-2020-323664 . hal-03846901

HAL Id: hal-03846901





<https://hal.science/hal-03846901>

Submitted on 11 Nov 2022

HAL is a multi-disciplinary open access archive for the deposit and dissemination of scientific research documents, whether they are published or not. The documents may come from teaching and research institutions in France or abroad, or from public or private research centers.

L'archive ouverte pluridisciplinaire **HAL**, est destinée au dépôt et à la diffusion de documents scientifiques de niveau recherche, publiés ou non, émanant des établissements d'enseignement et de recherche français ou étrangers, des laboratoires publics ou privés.

Gut mucosa alterations and loss of segmented filamentous bacteria in type 1 diabetes are associated with inflammation rather than hyperglycaemia

Matthieu Rouland ^{1,2}, Lucie Beaudoin,^{1,2} Ophélie Rouxel,^{1,2} Léo Bertrand ^{1,2}, Lucie Cagninacci,^{1,2} Azadeh Saffarian,³ Thierry Pedron,³ Dalale Gueddouri,¹ Sandra Guilmeau,¹ Anne-Françoise Burnol,¹ Latif Rachdi ¹, Asmaa Tazi,¹ Juliette Mouriès,^{4,5} Maria Rescigno,^{4,5} Nathalie Vergnolle,⁶ Philippe Sansonetti,³ Ute Christine Rogner,^{1,2} Agnès Lehuen ^{1,2}

► Prepublication history and additional material is published online only. To view please visit the journal online (<http://dx.doi.org/10.1136/gutjnl-2020-323664>).

For numbered affiliations see end of article.

Correspondence to

Professor Agnès Lehuen, Institut Cochin, Université de Paris, CNRS UMR 8104 and INSERM U1016, 123 Boulevard de Port-Royal, Paris 75014, France; agnes.lehuen@inserm.fr

MR, LB, OR and LB are joint first authors.

Received 19 November 2020

Revised 1 February 2021

Accepted 2 February 2021

Published Online First

16 February 2021

ABSTRACT

Objective Type 1 diabetes (T1D) is an autoimmune disease caused by the destruction of pancreatic β -cells producing insulin. Both T1D patients and animal models exhibit gut microbiota and mucosa alterations, although the exact cause for these remains poorly understood.

We investigated the production of key cytokines controlling gut integrity, the abundance of segmented filamentous bacteria (SFB) involved in the production of these cytokines, and the respective role of autoimmune inflammation and hyperglycaemia.

Design We used several mouse models of autoimmune T1D as well as mice rendered hyperglycaemic without inflammation to study gut mucosa and microbiota dysbiosis. We analysed cytokine expression in immune cells, epithelial cell function, SFB abundance and microbiota composition by 16S sequencing. We assessed the role of anti-tumour necrosis factor α on gut mucosa inflammation and T1D onset.

Results We show in models of autoimmune T1D a conserved loss of interleukin (IL)-17A, IL-22 and IL-23A in gut mucosa. Intestinal epithelial cell function was altered and gut integrity was impaired. These defects were associated with dysbiosis including progressive loss of SFB. Transfer of diabetogenic T-cells recapitulated these gut alterations, whereas induction of hyperglycaemia with no inflammation failed to do so. Moreover, anti-inflammatory treatment restored gut mucosa and immune cell function and dampened diabetes incidence.

Conclusion Our results demonstrate that gut mucosa alterations and dysbiosis in T1D are primarily linked to inflammation rather than hyperglycaemia. Anti-inflammatory treatment preserves gut homeostasis and protective commensal flora reducing T1D incidence.

INTRODUCTION

Type 1 diabetes (T1D) is an autoimmune disease characterised by the destruction of pancreatic β -cells that produce insulin.¹ The pathological activation of the immune system results in pancreatic inflammation, anti-islet antibody production, and islet infiltration by cytotoxic cells.^{2,3} Both innate and adaptive immune systems are inappropriately

Significance of this study

What is already known on this subject?

- Individuals affected by type 1 diabetes (T1D) exhibit an altered gut mucosa associated with increased intestinal permeability and a proinflammatory immune profile.
- Intestinal interleukin (IL)-17A and IL-22 participate in the maintenance of gut integrity and both can be induced by segmented filamentous bacteria (SFB) in the ileum.
- Gut microbiota of both diabetic and at-risk patients differs from that of healthy subjects.

What are the new findings?

- In non-obese diabetic mice, diabetes onset was associated with reduced IL-17A, IL-22 and IL-23A production in ileum, increased intestinal permeability and bacteria translocation.
- There was a progressive loss of SFB during disease development.
- Hyperglycaemia alone did not recapitulate gut mucosa and microbiota alterations occurring in autoimmune models of T1D.
- Anti-inflammatory treatment restored gut mucosa and immune cell function, and reduced diabetes development.

How might it impact on clinical practice in the foreseeable future?

- Our results reveal SFB as a potential biomarker of T1D progression in at-risk individuals and suggest that an anti-inflammatory treatment might be of interest to reduce intestinal alteration associated with T1D onset.

activated and involved in disease progression, in the pancreas and associated pancreatic lymph nodes (PLN).^{2,3} The resulting loss of insulin production leads to chronic hyperglycaemia and forces patients to rely on an insulin replacement therapy for life.¹

Another organ severely affected in T1D is the gastrointestinal tract. Several studies have described structural alterations of the gut



© Author(s) (or their employer(s)) 2022. No commercial re-use. See rights and permissions. Published by BMJ.

To cite: Rouland M, Beaudoin L, Rouxel O, et al. *Gut* 2022;**71**:296–308.

mucosa, such as a reduction in crypt length and tight junction proteins expression in both patients with T1D and animal models.^{4–9} Functional studies using mannitol-lactose clearance in patients with T1D and fluorescein isothiocyanate (FITC) dextran in animal models of T1D demonstrated that gut integrity is weakened, allowing an increased crossing of bacterial components from the gut lumen to systemic circulation.^{10–13} Several factors are suspected to be involved in gut permeability increase in the context of diabetes, including alimentation, microbiota alteration and enteric infection.^{8,14–17}

In parallel, the gut immune system, which resides in close contact with microbiota, displays proinflammatory features on T1D development.^{18–20} The incidence of chronic intestinal inflammation is higher in patients compared with the general population.^{21,22} Infiltration of proinflammatory cells is increased in the gut mucosa of T1D patients compared with healthy controls while Forkhead box P3⁺ (FOXP3⁺) regulatory T cells frequencies are reduced.^{18,19,23} We previously reported that mucosal-associated invariant T (MAIT) cells exert a key role in maintaining gut integrity that is lost during T1D progression in non-obese diabetic (NOD) mice.²⁴ Indeed, MAIT-deficient NOD mice develop an exacerbated disease associated with increased gut alterations and bacteria DNA translocation into PLN.²⁴ During disease progression in NOD females, MAIT cells lose interleukin (IL)-17A and IL-22 production, two critical cytokines required to maintain gut integrity.^{25–27}

Given that a variety of gut immune cells can produce IL-17A and IL-22, we examined whether the cytokine production loss, observed in MAIT cells, was extended to these other cells in the context of T1D. Since segmented filamentous bacteria (SFB) can induce the production of both cytokines and has been associated with T1D in mouse models, we investigated whether SFB was altered during diabetes development. Finally, using several different mouse models of diabetes we sought to determine the cause of gut and microbiota alterations in T1D. Our study reveals a concomitant loss of SFB, IL-17A, IL-22 and gut integrity during T1D progression and that gut inflammation, rather than hyperglycaemia, is an important driver of gut mucosa alteration and dysbiosis. Moreover, our results highlight the potential of treating gut inflammation to prevent diabetes.

RESULTS

T1D development in NOD mice is associated with decreased production of IL-17A, IL-22 and IL-23A by intestinal immune cells

We first began our investigation of gut alterations by analysing the production of cytokines in the *lamina propria* (LP) of ileum from female NOD mice at prediabetic stage (8–10 weeks) and at diabetes onset. A significant decrease in transcripts for *Il17a*, *Il22* and *Il23a* was observed in diabetic compared with younger prediabetic NOD mice (figure 1A). To confirm this decrease at the protein level, flow cytometry analyses of LP cells were performed. Intracellular labelling of IL-17A and IL-22 cytokines of haematopoietic cells (CD45⁺), T cell receptor (TCR)-β⁺ cells and TCR-β⁺ lymphoid cells also revealed a significant decrease in the frequency of IL-17A and IL-22-producing cells in diabetic mice (figure 1B,C). Similar reductions were observed in absolute cell numbers (online supplemental figure 1A,B).

Since the Retinoic-acid-receptor-related Orphan nuclear Receptor gamma (RORγt) is a key transcription factor controlling IL-17A²⁸ and IL-22 production,²⁷ we used a RORγt-Green Fluorescent Protein (GFP) reporter NOD mouse line that we had generated to evaluate RORγt cellular expression.²⁴ At the diabetic stage, an overall decrease of RORγt-GFP expression was observed in CD45⁺, TCRβ⁺ and TCRβ⁺ cells (figure 1D and online supplemental figure 1C). Moreover, we observed the same decrease in CD4 T, invariant Natural Killer T (iNKT), MAIT, γδT and innate lymphoid cells (online supplemental figure 1D). These data show that T1D development is associated with a general defect in IL-17A and IL-22 production by gut mucosa immune cells.

T1D development is associated with alteration of gut mucosa functions and decreased SFB abundance

The fucosyltransferase 2 (FUT2) enzyme expressed by gut epithelial cells (ECs) is representative of a protective mechanism promoting the maintenance of the commensal gut microbiota, protecting the host against opportunistic pathogens.²⁹ Since IL-22 can induce *Fut2* expression by ileum ECs, we analysed *Fut2* expression in the ileum of female NOD mice at different disease stages.^{29,30} mRNA expression of *Fut2* in ileum of diabetic mice was significantly lower than in younger prediabetic mice (figure 2A). In addition, analysis of α(1,2)-fucose levels on EC surface by the binding of fluorescent Ulex europaeus agglutinin-1 (UEA-1) lectin showed a significant decrease in the frequency and intensity of EC fucosylation in diabetic mice (figure 2B).

Since SFB is intimately attached to ECs in ileum and induce IL-17A and IL-22 production by gut immune cells,^{31–36} we investigated whether ECs alterations were associated with a loss of SFB. The relative abundance of SFB in ileum was significantly reduced in diabetic mice compared with prediabetic mice (figure 2C). The decrease of SFB relative quantities in diabetic mice was also observed in faeces (figure 2D). Analysis revealed that SFB levels progressively decreased from 4 weeks up to 13 weeks old female NOD mice free from diabetes (figure 2E). Progressive loss of SFB was similar between age-matched female C57BL/6J and female NOD mice that remained diabetes-free until up to 13 weeks of age. However, SFB loss was significantly increased as soon as 9 weeks of age in female NOD mice that became subsequently diabetic at 13 weeks of age (figure 2F). Of note, SFB relative quantity in faeces stabilised at diabetes onset. The diminished amount of SFB in ileum positively correlated with the decreased expression of *Fut2* mRNA in diabetic mice (figure 2G).

After oral gavage, blood FITC-dextran concentration was significantly higher in diabetic NOD mice than in 10-week-old NOD mice (figure 2H). We also observed a reduction of claudin-4 (*Cldn4*), tight junction protein 1 (*Tjp1*), occludin (*Ocln*) and mucin-2 (*Muc2*) mRNA in sorted epithelial cell adhesion molecule (EpCam)⁺ ECs of ileum from diabetic compared with younger mice (figure 2I).

We next analysed whether loss of gut integrity in diabetic mice was associated with bacterial translocation. Increased detection of 16S DNA was observed in liver of diabetic NOD mice compared with prediabetic NOD and C57BL/6J mice (figure 2J). There was also an increase of CFU of anaerobic and aerobic bacteria in liver from 17-week-old and diabetic mice compared with younger NOD and control C57BL/6J

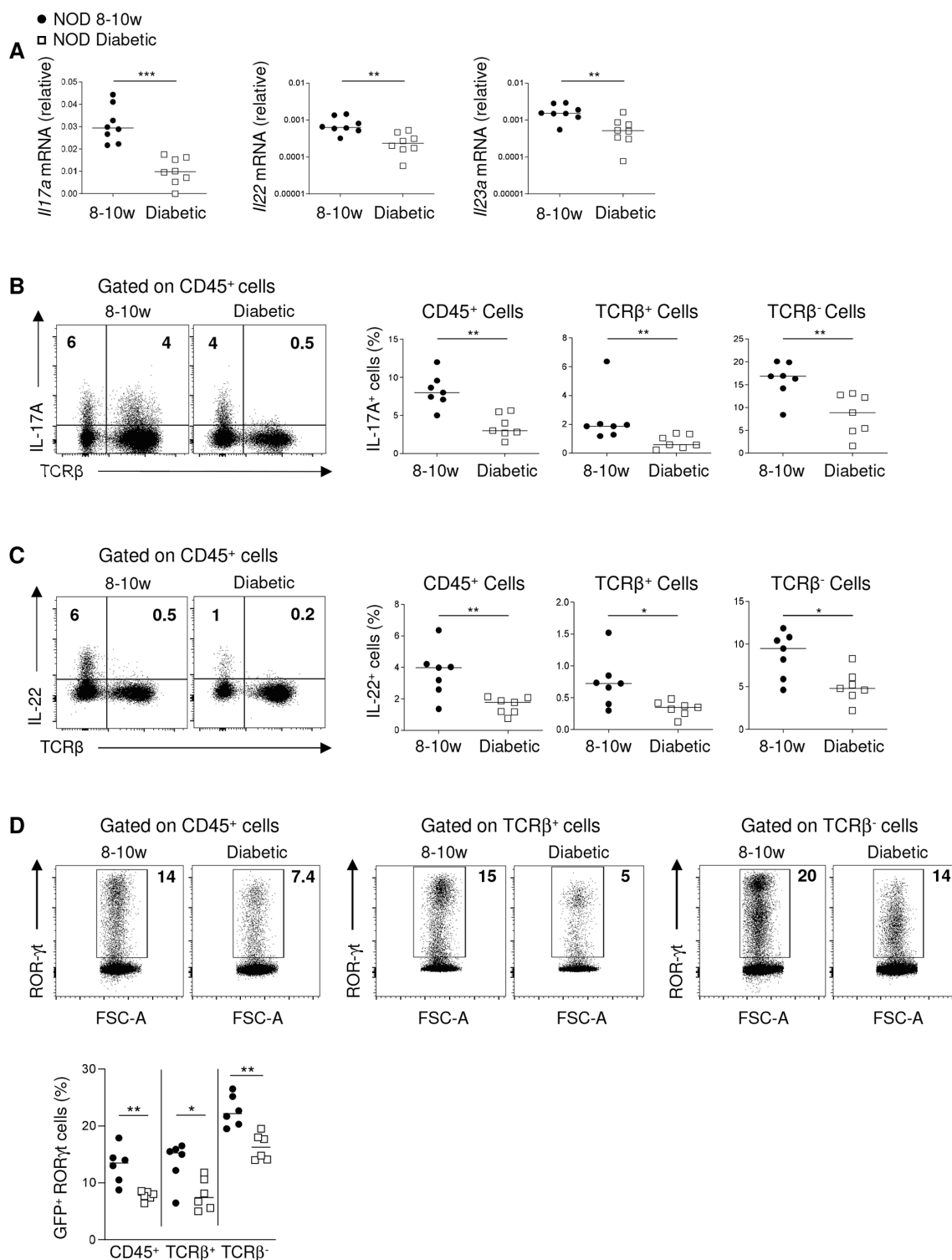


Figure 1 Decreased IL-17A and IL-22 cytokine production in the gut mucosa of diabetic NOD mice. *Lamina propria* (LP) cells from small intestine (ileum) of prediabetic (8–10 weeks) and diabetic females NOD mice were analysed. (A) RT-qPCR of *Il17a*, *Il22* and *Il23a* mRNA in ileum of NOD mice (n=8 mice per group). Results were normalised to the expression of the reference gene *Gapdh*. (B, C) Mice were stimulated for 2 hours in vivo by injection of flagellin. Activated LP cells were analysed by flow cytometry. Representative dot plots and percentages of IL-17A⁺ cells (B) and IL-22⁺ cells (C) among CD45⁺, TCRβ⁺ or TCRβ⁻ lymphoid cells are shown (n=7 mice per group). (D) Flow cytometry analysis of RORγt-GFP expression by LP cells in RORγt-GFP NOD mice. Representative dot plots and percentages of RORγt-GFP⁺ cells among CD45⁺, TCRβ⁺ or TCRβ⁻ lymphoid cells are shown (n=6 mice per group) according to cell size (FSC-A). Data are representative of two or three independent experiments and small horizontal lines indicate the median, each data point represents one individual mouse. *P<0.05, **p<0.01 and ***p<0.001 (two-tailed Mann-Whitney U test). FSC-A, forward scatter-area; GFP, green fluorescent protein; IL, interleukin; NOD, non-obese diabetic; ROR, Retinoic-acid-receptor-related Orphan nuclear Receptor; TCR, T-cell receptor.

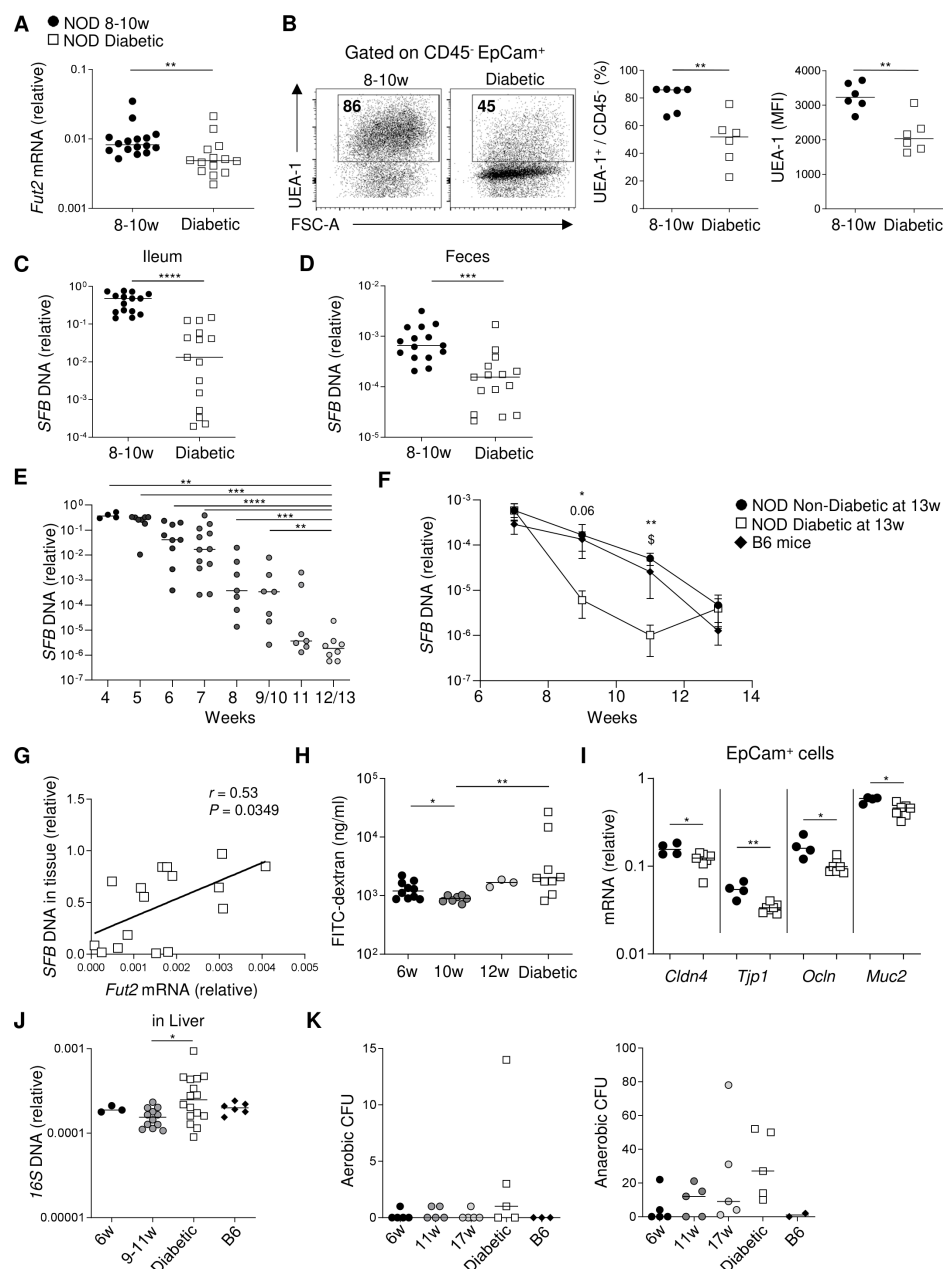


Figure 2 T1D development in NOD mice is associated with altered epithelial cells (ECs) function and decreased SFB level. LP cells from small intestine (ileum) of prediabetic (8–10 weeks) and diabetic females NOD mice were analysed. (A) Relative mRNA expression of fucosyltransferase 2 (*Fut2*) in ileum (n=14–16 mice per group). Results were normalised to the expression of the reference gene *Gapdh*. (B) ECs from small intestine (ileum) were analysed (n=6 mice per group). Flow cytometry analysis of intestinal ECs (CD45⁺ EpCam⁺) was performed with UEA-1-FITC lectin to detect fucosylated-ECs. Representative dot plots, percentages and mean fluorescence intensity (MFI) of fucosylated ECs are shown according to cell size (FSC-A). (C, D) Ileal tissues and faecal content were collected and extracted DNA was analysed by qPCR for the presence of intestinal SFB (n=15 mice per group). (E) SFB level was assessed by qPCR in faeces from non-diabetic NOD mice from 4 to 13 weeks of age (n=4–12 mice per group). (F) SFB level was quantified by qPCR and followed from 7 weeks to 13 weeks of age in faeces from female C57BL/6J mice, female NOD mice that became, or not, diabetic at 13 weeks of age (n=4–15 mice per group). Significant differences between C57BL/6J and diabetic NOD mice are represented by a \$ symbol. (G) Spearman's correlation between SFB level and *Fut2* relative expression in ileal tissues (n=16 diabetic mice). (H) Intestinal gut permeability measured by in vivo FITC-dextran assay in NOD mice at 6, 10, 12 weeks of age and at diabetes onset (n=3–10 mice per group). (I) RT-qPCR analysis of claudin 4 (*Cldn4*), tight junction protein 1 (*Tjp1*), occludin (*Ocln*), mucin 2 (*Muc2*) mRNA in EpCam⁺ cells from ileum of female NOD mice (n=4–7 mice per group). Results were normalised to the expression of *Gapdh*. (J) 16S bacterial DNA level from the liver was assessed by qPCR from 6 to 11 weeks of age NOD mice, diabetic NOD mice and C57BL/6J mice (n=3–16 per group). (K) Livers were recovered in aseptic conditions from NOD mice at different ages and C57BL/6J control mice (n=2–5 mice per group). Liver cells were lysed and then plated on Terrific broth agar plates at 37°C in aerobic or anaerobic conditions to evaluate bacterial dissemination. The number of CFU was assessed after a 24-hour (aerobic) or 48-hour (anaerobic) incubation period. SFB levels were normalised to the respective abundance of total bacteria. Data are representative from at least two independent experiments and horizontal lines indicate the median, each data point represents an individual mouse. */\$P<0.05, **p<0.01, ***p<0.001, ****p<0.0001 (two-tailed Mann-Whitney U test). FITC, Fluorescein isothiocyanate; FSC-A, forward scatter-area; LP, lamina propria; NOD, non-obese diabetic; SFB, segmented filamentous bacteria; T1D, type 1 diabetes; UEA-1, ulex europaeus agglutinin-1.

mice (figure 2K). Bacteria analysis highlighted that bacteria of anaerobic and aerobic culture from the liver were mostly *Lactobacillus murinus* (online supplemental table 1). Together these data show that progression toward diabetes in NOD mice is associated with several gut mucosa alterations and a dramatic decrease of SFB.

Gut mucosa alterations in streptozotocin-induced diabetes in NOD and C57BL/6J mice

We next investigated whether the observed gut mucosa alterations and SFB loss were restricted to T1D development in NOD mice or could be observed in other T1D mouse models. A commonly used mouse model of T1D is based on treatment with multiple low doses of streptozotocin (STZ)³⁷ (figure 3A). NOD males became diabetic shortly after STZ treatment and harboured the same mucosa alterations as spontaneous diabetic NOD females: notably reduced *Il17a*, *Il22* and *Il23a* mRNA expression in LP cells of ileum (figure 3B), a significant decrease of UEA-1⁺ ECs frequencies (figure 3C) as well as a reduction of *Fut2* mRNA transcription (figure 3D) and diminished levels of SFB in faeces associated with treatment duration (figure 3E). To exclude the possibility of NOD mouse-specific defects we also analysed C57BL/6J mice treated with STZ (figure 3F). As in diabetic NOD mice, diabetes in STZ-treated C57BL/6J mice was associated with reduced transcripts for *Il17a*, *Il22* and *Il23a* in LP cells of ileum (figure 3G), decreased frequencies of UEA-1⁺ ileum ECs, as well as a slight decrease of mean fluorescence intensity of UEA-1 ($p=0.0519$) (figure 3H). We observed decreased levels of SFB in ileum and faeces as in NOD mice (figure 3I). Therefore, these gut microbiota and mucosa alterations seem to represent common features associated with T1D onset.

Hyperglycaemia does not replicate intestinal alterations observed in T1D

Next, we investigated whether these alterations observed in diabetic mice could occur on induction of hyperglycaemia in absence of autoimmune/inflammatory reaction. To this end, C57BL/6J mice were grafted with a pump allowing continuous diffusion of S961, an insulin receptor antagonist³⁸ (figure 4A). In contrast to what was observed in prediabetic NOD and STZ-treated mice, hyperglycaemia in S961-treated mice induced a significant increase of SFB abundance in faeces and ileum (figure 4B). Moreover, there was no difference in UEA-1 expression on intestinal ECs and no modification of *Il17a* and *Il22* mRNA expression in cells from ileum LP (figure 4C,D). However, hyperglycaemia induced a significant increase of *Il23a* mRNA expression in LP cells from ileum (figure 4D). These data show that hyperglycaemia alone does not induce SFB, IL-17A, IL-22 and IL-23A loss that we observed in NOD and STZ-treated mice.

Diabetes induced by diabetogenic T-cells alters intestinal homeostasis and SFB level

We transferred by intravenous injection diabetogenic T cells (BDC2.5) in *Trac*^{-/-} NOD recipient mice. This model allows synchronisation of T1D induction and monitoring of diabetogenic CD4⁺ T cells migration within different tissues. Onset of diabetes in recipient mice (figure 5A) was associated with the same gut alterations as observed in NOD mice such as a significant decrease of SFB in ileum and faeces (figure 5B), an enhanced gut permeability evaluated

by FITC-dextran in blood after oral gavage (figure 5C), and a decrease in mRNA transcripts for *Il17a*, *Il22* and *Il23a* in cells from ileum (figure 5D). Increased gut permeability in diabetic recipient mice was associated with a significant decrease of *Tjp1* and *Muc2* mRNA levels and a slight reduction of *Cldn4* ($p=0.07$) and *Ocln* ($p=0.10$) mRNA levels in intestinal ECs (figure 5E).

We next assessed whether diabetogenic BDC2.5 T cells could home into the ileum of recipient mice. Flow cytometry analysis showed presence of BDC2.5 T cells from day 2 to day 13 in the ileum, PLN and mesenteric lymph nodes (MLN) (figure 5F,G and online supplemental figure 2). BDC2.5 T cell frequency in ileum was higher at day 13 compared with MLN and PLN (figure 5F,H). Furthermore, an elevated frequency of BDC2.5 T cells in ileum produced interferon (IFN)- γ and tumour necrosis factor (TNF) α compared with MLN and PLN (figure 5I,J). We also transferred BDC2.5 T cells in wild-type NOD recipient mice, in which they do not induce diabetes,³⁹ allowing analysis of BDC2.5 T cell behaviour without potential contribution of homeostatic proliferation that could occur in *Trac*^{-/-} NOD recipient mice. Flow cytometry analysis confirmed the presence of BDC2.5 T cells at day 8 in ileum, MLN, PLN and pancreatic islets (figure 5K,L and online supplemental figure 3AB). Increased frequency of BDC2.5 T cells in these organs resulted from their higher proliferation rate compared with host CD45.2⁺ CD4⁺ T cells (figure 5M and online supplemental figure 3C-E). Moreover, BDC2.5 T cells produced high levels of IFN- γ and TNF α in ileum, MLN and PLN compared with host CD45.2⁺ CD4⁺ T cells and the highest TNF α level in BDC2.5 T cells was observed in ileum even when compared with all organs, including pancreatic islets (figure 5N,O and online supplemental figure 3FG). These data suggest that gut mucosa alterations in recipient mice are caused by diabetogenic T cell production of inflammatory cytokines in ileum.

Gut microbiota alteration in NOD mice matches the observations in BDC2.5 model

As our data revealed the impact of gut inflammation on SFB levels, we next performed a more extensive analysis of gut microbiota alterations in mouse models of T1D versus our non-autoimmune hyperglycaemic mouse model. 16S ribosomal DNA sequencing confirmed SFB reduction with T1D progression in NOD mice at different ages as well as in BDC2.5 T cell recipient mice (figure 6A). 16S DNA sequencing also confirmed the increase of SFB in hyperglycaemic S961-treated mice (figure 6A). Principal component analysis (PCA) of 16S ribosomal DNA sequencing showed an unsupervised overview of gut microbiota modification in these mice (figure 6B). In NOD mice, there was a shift of the gut microbiome from 6-week-old to 10-week-old mice to diabetic mice with the PC2 (9.85%). In BDC2.5 T cell transfer experiments, two clusters separated control from BDC2.5 T cell-induced diabetic mice mostly by PC2 (20.23%) (figure 6B). Lastly, in S961 experiments we observed two clusters that separated control from hyperglycaemic mice mostly by PC1 (34.05%) (figure 6B).

We next explored more precisely gut microbiota modifications during T1D progression in NOD mice. 16S sequencing of faecal content from NOD mice from 6 weeks of age to diabetes onset showed a total of 24 phyla and genera modifications (figure 6C and online supplemental figure 4). As previously shown, relative abundance of *Bacteroidetes* and *Firmicutes* were, respectively,

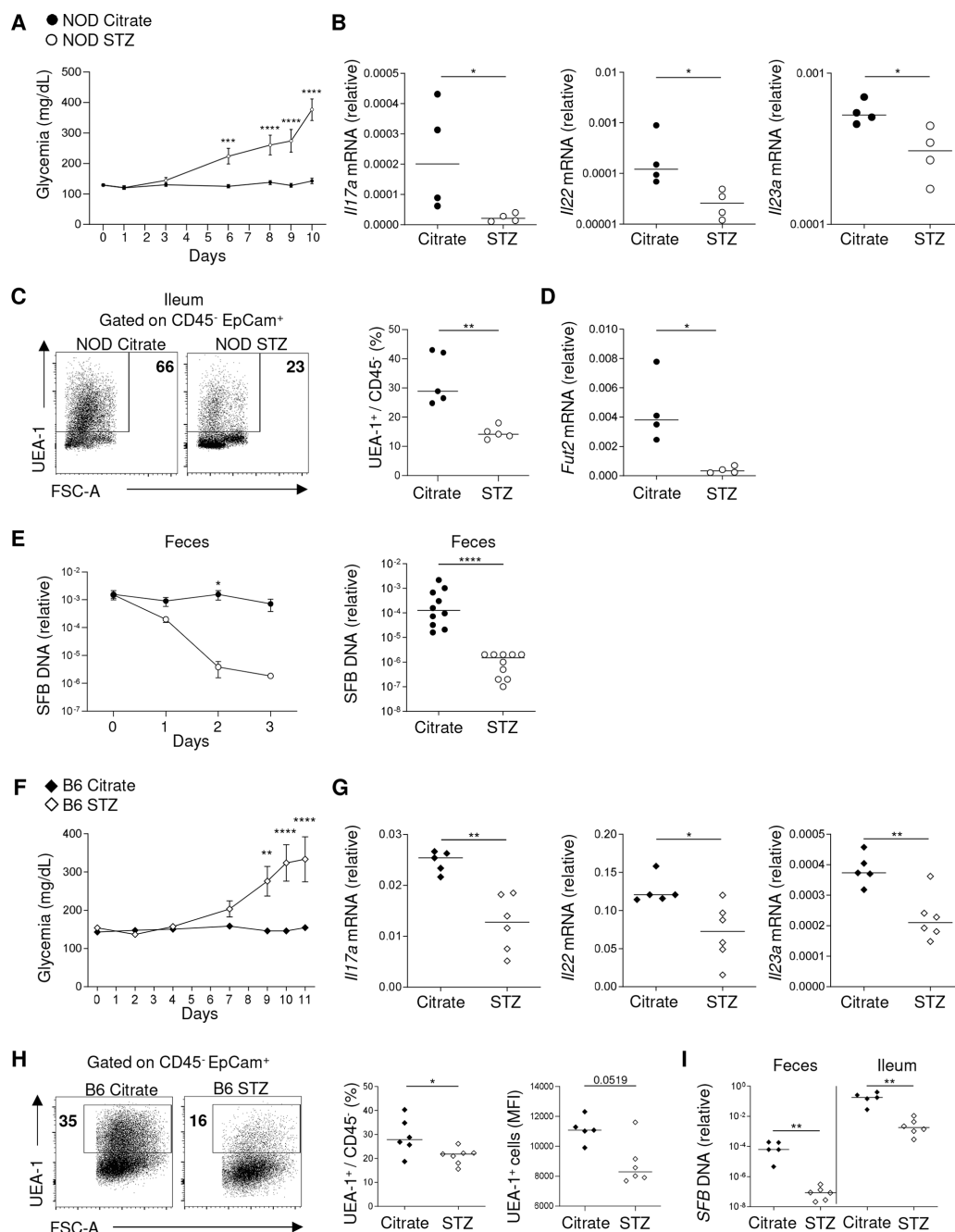


Figure 3 Modification of gut mucosa homeostasis in streptozotocin (STZ)-induced diabetes in NOD and C57BL/6J mice. Male NOD and C57BL/6J mice received three low doses (50 mg/kg) of STZ during three following days, starting on day 0, to induce diabetes, control mice received citrate buffer injection only. (A) NOD mice treated with STZ were monitored with daily measurement of blood glucose concentration (mg/dL) ($n=6-15$ mice per day and group). (B) RT-qPCR analysis of *Il17a*, *Il22* and *Il23a* mRNA from ileum LP of NOD mice on day 10 after treatment or not with STZ ($n=4$ mice per group). Results were normalised to the expression of *Gapdh*. (C) Flow cytometry analysis of intestinal ECs (CD45⁺ EpCam⁺) was performed with UEA-1-FITC to detect fucosylated-ECs. Representative dot plots and percentages of fucosylated ECs are shown ($n=5$ mice per group) according to cell size (FSC-A). (D) Relative expression of *Fut2* in ileum 10 days after STZ injection ($n=4$ mice per group). Results were normalised to the expression of *Gapdh*. (E) SFB level was assessed daily by qPCR analysis in faeces of STZ treated mice from day 0 to day 3 ($n=6$ mice per group) and on day 10 ($n=10$ mice per group). Results were normalised to the respective abundance of total bacteria. (F) C57BL/6J mice treated with STZ were monitored with daily measurement of blood glucose concentration (mg/dL) ($n=5-6$ mice per group). (G) RT-qPCR analysis of *Il17a*, *Il22* and *Il23a* mRNA from ileum LP of C57BL/6J mice treated or not with STZ on day 11 post-treatment start ($n=5-6$ mice per group). Results were normalised to the expression of *Gapdh*. (H) Flow cytometry analysis of intestinal ECs (CD45⁺ EpCam⁺) was performed with UEA-1-FITC to detect fucosylated-ECs. Representative dot plots, percentages, and mean fluorescence intensity (MFI) of fucosylated-ECs are shown ($n=5-7$ mice per group) according to cell size (FSC-A). (I) SFB level was assessed by qPCR analysis in faeces and ileum on day 11 (day of sacrifice) ($n=5-6$ mice per group). Results were normalised to the respective abundance of total bacteria. Data are representative of at least two independent experiments and horizontal lines indicate the median, each data point represents one individual mouse. * $P<0.05$, ** $p<0.01$, *** $p<0.001$ and **** $p<0.0001$ (two-tailed Mann-Whitney U test). ECs, epithelial cells; EpCam, EC adhesion molecule; FSC-A, forward scatter-area; IL, interleukin; LP, lamina propria; NOD, non-obese diabetic; SFB, segmented filamentous bacteria; UEA, ulex europaeus agglutinin-1.

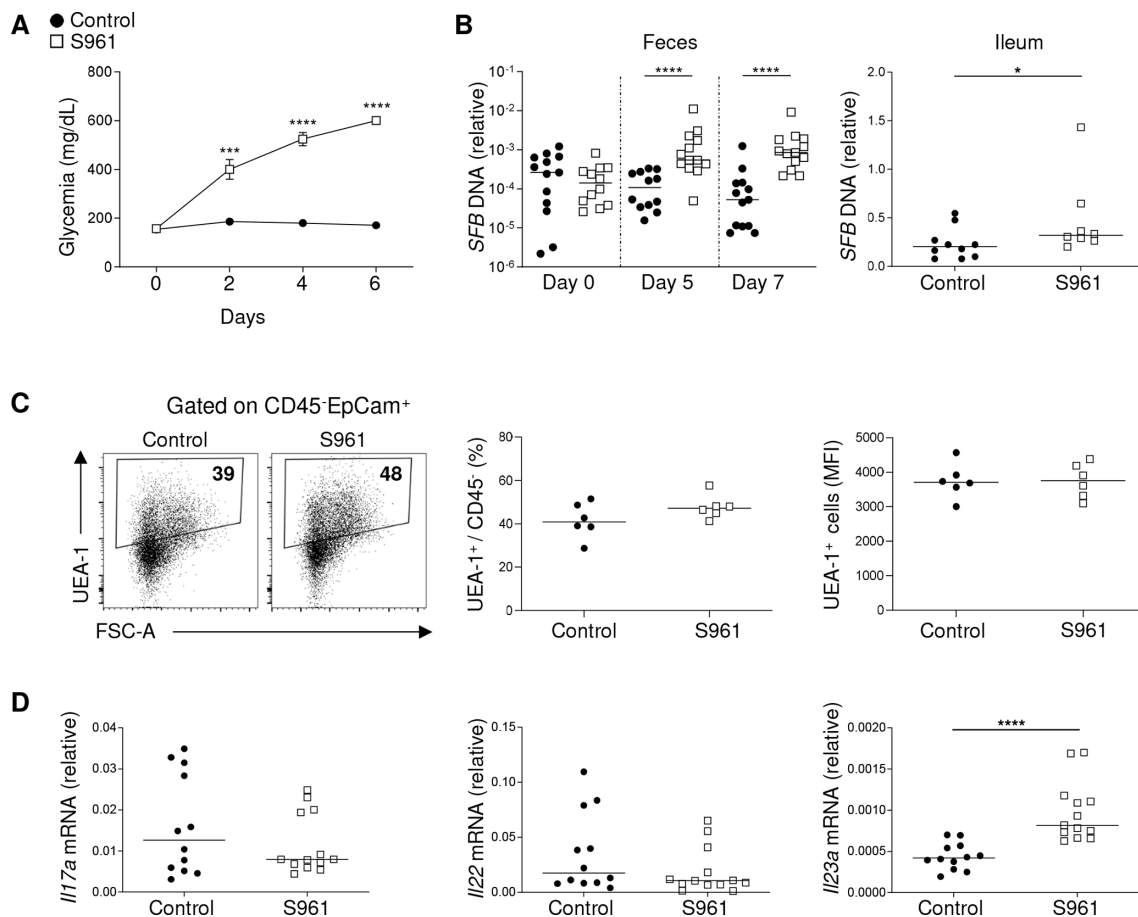


Figure 4 Hyperglycaemia does not replicate intestinal alteration observed during T1D progression. Hyperglycaemia was induced by a continuous administration of S961, an antagonist of insulin receptor molecule at 20 nmol/week with a flow rate of 0.5 μ L/hour for 7 days, and PBS was used for control mice. (A) Mice were monitored with measurement of blood glucose level (mg/dL) every 48 hours. Glycaemia kinetic representative of one experience among all (n=4 mice per group). (B) Relative SFB levels were analysed by qPCR in faeces on day 0 (before pump graft), 5 and 7, and in ileum after sacrifice on day 7 (n=8–13 mice per group). Results were normalised to the respective abundance of total bacteria. (C) Flow cytometry analysis of intestinal ECs (CD45⁺ EpCam⁺) was performed with UEA-1-FITC to detect fucosylated-ECs. Representative dot plots, percentages and mean fluorescence intensity (MFI) of fucosylated ECs are shown (n=6 mice per group) according to cell size (FSC-A). (D) RT-qPCR analysis of *Il17a*, *Il22* and *Il23a* mRNA in LP of ileum on day 7 (n=12–13 mice per group). Results were normalised to the expression of *Gapdh*. Data are representative of at least three independent experiments and horizontal lines indicate the median, each data point represents one individual mouse. *P<0.05, ***p<0.001, ****p<0.0001 (two-tailed Mann-Whitney U test). ECs, epithelial cells; EpCam, EC adhesion molecule; FSC-A, forward scatter-area; IL, interleukin; LP, lamina propria; SFB, segmented filamentous bacteria; T1D, type 1 diabetes; UEA, ulex europaeus agglutinin-1.

decreased and increased in diabetic NOD mice as compared with prediabetic mice.⁴⁰ We further observed other modifications during T1D progression in NOD mice and several were common with modifications occurring in BDC2.5 T cell recipient mice that became diabetic. A significant increase of *Coproccoccus*, *Dorea*, *Oscillospira*, *Thiobacter* was associated with disease progression (figure 6C,D). However, other gut microbiota modifications were similar during the development of diabetes in NOD mice and induction of hyperglycaemia in S961-treated mice. In both mouse models, there was a significant decrease of *Bacteroidetes* phylum and an increase of *Bacteroides* genus. Conversely, *Parabacteroides* was reduced in hyperglycaemic mice compared with diabetic NOD mice (figure 6C,E). We did not observe any similarities in microbiome alteration between BDC2.5 T cell-transferred mice and hyperglycaemic S961-treated mice (figure 6D,E and online supplemental figure 5). Some modifications only occurred in S961-treated mice such as an increase of *Enterococcus*, *Erwinia* and *Klebsiella* and a decrease of *Allobaculum* genera (figure 6E). While *Coproccoccus* increased in diabetic NOD mice and BDC2.5 T cell-transferred mice, this genus was

rather reduced (p=0.0642) in hyperglycaemic S961-treated mice compared with their controls (figure 6E). Similarly, the increase of *Dorea* and *Oscillospira* genera in both diabetic NOD mice and BDC2.5 T cell-transferred mice was not observed in hyperglycaemic S961-treated mice. Overall, these data highlight several gut microbiota modifications occurring in two mouse models of autoimmune diabetes but not on induction of hyperglycaemia.

Anti-TNF α treatment prevents gut mucosa alterations, restores SFB levels and prevents T1D onset

Since transferred BDC2.5 diabetogenic T cells migrated and expanded to the ileum where they produced a large amount of TNF α , we assessed the impact of Remicade, an anti-TNF α antibody (Infliximab), on gut inflammation and diabetes development. Anti-TNF α antibody treatment had a major impact on gut mucosa as it increased *Il17a* and *Il22* mRNA levels as well as *Foxp3* transcript abundance in LP cells of ileum from treated mice compared with isotype-injected control mice (figure 7A). Ileal EC function was improved by anti-TNF α treatment as UEA-1

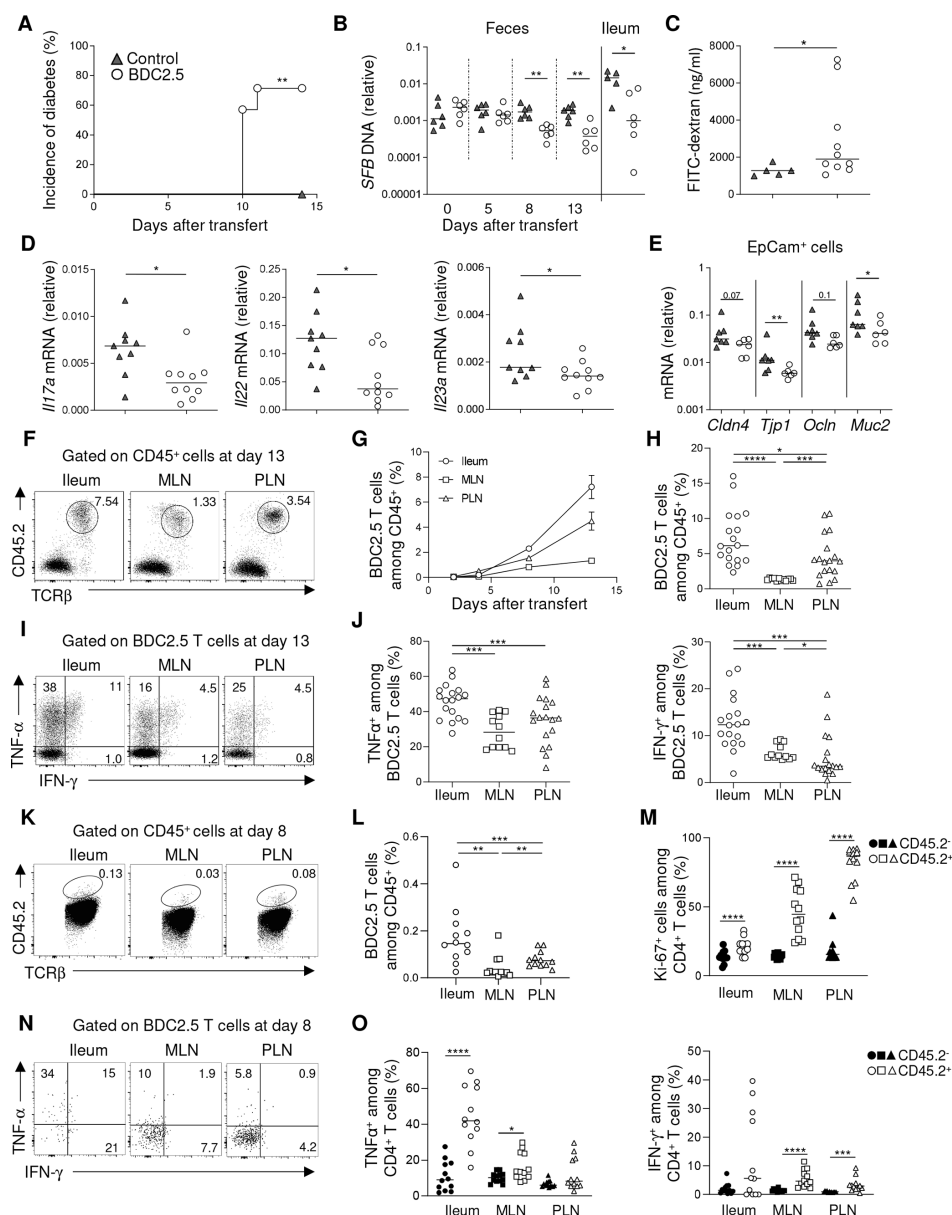


Figure 5 Transfer of BDC2.5 T cells impacts small intestine homeostasis. Diabetes was induced by intravenous injection of CD45.2⁺ CD4⁺ CD62L⁺ T cells from BDC2.5 *Trac*^{-/-} NOD mice into CD45.1⁺ *Trac*^{-/-} NOD recipient mice. Ileum, MLN, PLN and faecal pellets from NOD recipients and non-injected mice were collected and analysed. (A) Incidence of diabetes of recipient *Trac*^{-/-} NOD mice after transfer with BDC2.5 T cells (n=7 mice per group). (B) Relative SFB abundance was analysed by qPCR in faeces (on day 0, 5, 8 and 13) or in ileum (after sacrifice on day 13) (n=5–6 mice per group). Results were normalised to the respective abundance of total bacteria. (C) Intestinal gut permeability evaluated by in vivo FITC-dextran assay in recipient mice and their controls (n=5–10 per group). (D) On day 13, mice were sacrificed and the relative expression of *Il17a*, *Il22* and *Il23a* mRNA in LP of ileum were analysed by RT-qPCR (n=9–10 mice per group). Results were normalised to the expression of *Gapdh*. (E) RT-qPCR analysis of mRNA encoding for *Cldn4*, *Tjp1*, *Ocln*, *Muc2* in sorted ECs from ileum (n=6–7 mice per group). Results were normalised to the expression of *Gapdh*. (F, G) Representative dot plots and evolution of BDC2.5 T cells frequency among CD45⁺ cells in ileum, MLN, and PLN at day 2, 4, 8 and 13 after BDC2.5 T cell transfer into *Trac*^{-/-} NOD recipient mice (n=3–18 mice per group). (H) Frequencies of CD45.2⁺ TCRβ⁺ BDC2.5 T cell among CD45⁺ cells in ileum, MLN and PLN of *Trac*^{-/-} NOD recipient mice at day 13 after BDC2.5 T cell transfer (n=12–18 mice per group). (I, J) Representative dot plots and frequencies of cytokine production (IFN-γ and TNFα) among BDC2.5 T cells stimulated by PMA/ionomycin in ileum, MLN, and PLN on day 13 after BDC2.5 T cell transfer into *Trac*^{-/-} NOD recipient mice (n=12–18 mice per group). (K–O) Proliferation and cytokines secretion were analysed in CD45.1⁺ NOD mice ileum, MLN and PLN after intravenous injection of CD45.2⁺ CD4⁺ CD62L⁺ T cells from BDC2.5 *Trac*^{-/-} mice. (K–L) Representative dot plots and frequencies of CD45.2⁺ TCRβ⁺ BDC2.5 T cell frequencies among CD45⁺ cells at day 8 after BDC2.5 T cell transfer into NOD mice (n=12 mice per group). (M) Frequency of Ki-67⁺ cells in CD45.2⁺ or CD45.2⁻ cells among CD4⁺ cells in ileum, MLN and PLN at day 8 after BDC2.5 T cell transfer in NOD mice (n=12 mice per group). (N, O) Representative dot plots and frequencies of TNFα and IFN-γ expression in CD45.2⁺ BDC2.5 or CD45.2⁻ cells among CD4⁺ T cells in ileum, MLN, and PLN at day 8 after BDC2.5 T cell transfer in NOD mice (n=12 mice per group). Data are representative of at least two independent experiments and horizontal lines indicate the median, each data point represents one individual mouse for transferred *Trac*^{-/-} NOD recipient mice and two pooled mice for transferred NOD recipient mice. *P<0.05, **p<0.01, ***p<0.001, ****p<0.0001 (two-tailed Mann-Whitney U test). IFN-γ, interferon-γ; LP, lamina propria; MLN, mesenteric lymph nodes; NOD, non-obese diabetic; PLN, pancreatic lymph nodes; SFB, segmented filamentous bacteria; TCR, T cell receptor; TNFα, tumour necrosis factor α.

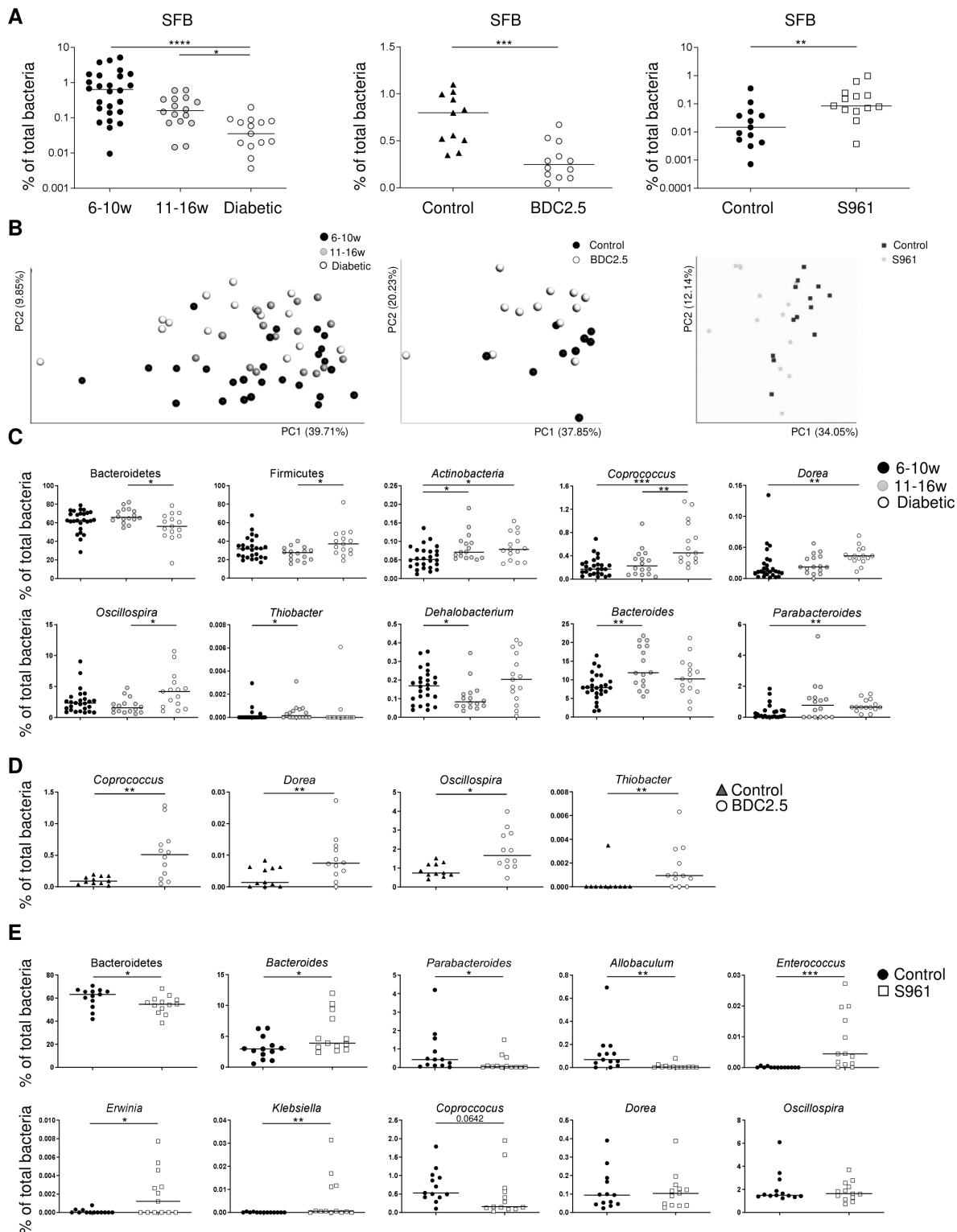


Figure 6 Gut microbiota composition of mice with autoimmune diabetes or metabolic-mediated hyperglycaemia. Microbiota composition was determined by 16S bacterial DNA sequencing of faeces from three groups of NOD mice at 6–10 weeks, 11–16 weeks and diabetic stages, C57BL/6J mice grafted with S961-containing pumps, and recipient *Trac*^{-/-} NOD mice transferred with BDC2.5 T cells, models respectively described in figures 4 and 5). (A) Percentages of SFB among total bacteria in faeces of NOD mice, BDC2.5 T cell recipient mice or PBS-treated and C57BL/6J mice grafted with S961- or PBS-containing pumps (n=11–26 mice per group). (B) Principal component analysis (PCA) plot highlighting 16S-sequenced gut microbiota differences of the respective groups in the three different mouse models. (C) Detailed analysis of the bacterial phyla and genera during T1D development in NOD mice (n=14–26 mice per group). (D) Detailed analysis of the bacterial phyla and genera in recipient mice after BDC2.5 T cell transfer or not in *Trac*^{-/-} NOD mice (n=11–13 mice per group). (E) Detailed analysis of the bacterial phyla and genera after hyperglycaemia induction or not in C57BL/6J mice (n=13 mice per group). Horizontal lines indicate the median, each data point represents one individual. *P<0.05, **p<0.01, ***p<0.001, ****p<0.0001 (Kruskal-Wallis test with Dunn's Multiple Comparison post-test or two-tailed Mann-Whitney U test). NOD, non-obese diabetic; SFB, segmented filamentous bacteria.

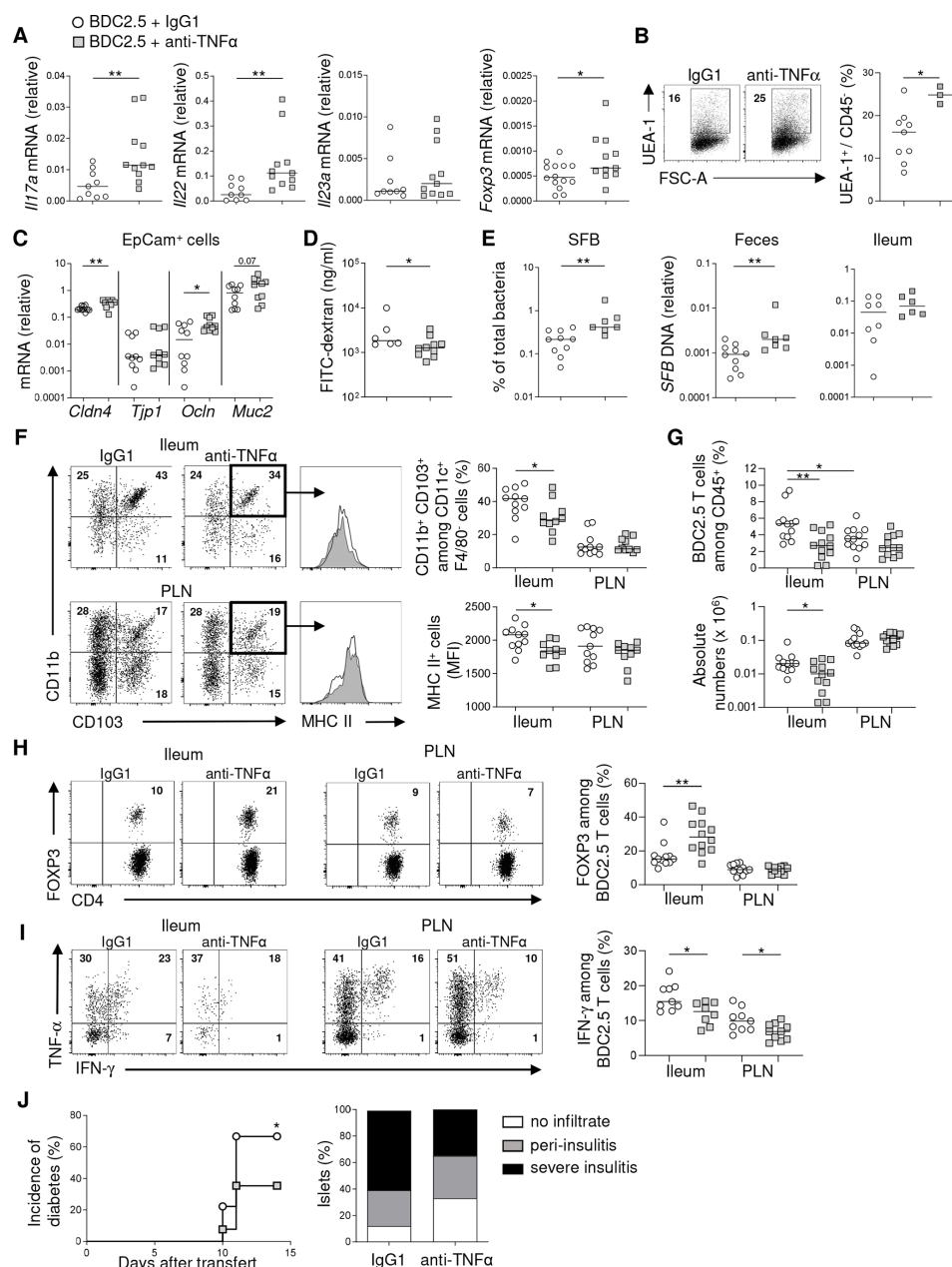


Figure 7 Anti-TNF α treatment prevents gut mucosa alteration and diabetes onset. Recipient CD45.1⁺ *Trac*^{-/-} NOD mice were transferred with 0.5×10^6 CD45.2⁺ CD4⁺ CD62L⁺ BDC2.5 T cells and treated with anti-TNF α (10 mg/kg) or human control IgG1 antibodies on day 0, 3, and 6. (A) RT-qPCR analysis of mRNA encoding for *Il17a*, *Il22*, *Il23a* and *Foxp3* from LP cells ($n=9-11$ mice per group). Results were normalised to the expression of *Gapdh*. (B) Flow cytometry analysis of intestinal ECs (CD45⁺ EpCam⁺) was performed with UEA-1-FITC to detect fucosylated-ECs. Representative dot plots and percentages of fucosylated-ECs are shown ($n=3-9$ mice per group) according to cell size (FSC-A). (C) RT-qPCR analysis of mRNA encoding for *Cldn4*, *Tjp1*, *Ocln* and *Muc2* in sorted ECs from ileum ($n=10$ mice per group). Results were normalised to the expression of *Gapdh*. (D) Intestinal gut permeability was evaluated with in vivo FITC-dextran assay ($n=6-10$ mice per group). (E) Relative SFB abundance and level determined by 16S-sequencing and qPCR of faecal contents and ileum tissue on day 13 post-transfer ($n=6-10$ mice per group). qPCR results were normalised to the respective abundance of total bacteria. (F) Mice were sacrificed on day 13 and ileum and pancreatic lymph nodes (PLN) were collected and analysed. Frequency of CD11b⁺ CD103⁺ DCs among CD11c⁺ F4/80⁺ cells and mean fluorescence intensity (MFI) of MHC class II on these CD11b⁺ CD103⁺ DCs in PLN and ileum from recipient mice treated with anti-TNF α or human control IgG1 antibodies ($n=10-11$ mice per group). (G) Absolute number and frequency of BDC2.5 T cells in ileum and PLN of recipient mice treated with anti-TNF α or human control IgG1 antibodies ($n=12$ mice per group). (H, I) Representative dot plots and frequencies of FOXP3 expression in BDC2.5 T cells and IFN- γ and TNF α cytokine expression in PMA ionomycin activated BDC2.5 T cells in PLN and ileum on day 13; after BDC2.5 T cell transfer into recipient mice treated with anti-TNF α or human control IgG1 antibodies ($n=8-12$ mice per group). (J) Analysis of pancreatic islet infiltration and incidence of diabetes of recipient *Trac*^{-/-} NOD mice on day 15 after transfer with BDC2.5 T cells and treatment with either anti-TNF α or human control IgG1 antibodies ($n=26-27$ mice per group). All data are representative of at least three independent experiments and horizontal lines indicate the median, each data point represents an individual mouse. * $P<0.05$, ** $p<0.01$ (unpaired t-test (in panel A), for *Foxp3* mRNA) and two-tailed Mann-Whitney U test). FSC-A, forward scatter-area; IFN- γ , interferon- γ ; LP, lamina propria; NOD, non-obese diabetic; PLN, pancreatic lymph nodes; SFB, segmented filamentous bacteria; TNF α , tumour necrosis factor α ; UEA-1, ulex europaeus agglutinin-1.

expression on intestinal ECs increased (figure 7B). In addition, transcript levels coding for *Cldn4*, *Ocln* were significantly elevated, with a slight increase of *Muc2* mRNA level ($p=0.07$), and gut permeability was significantly decreased (figure 7C,D). This was associated with an increase of SFB frequencies and relative quantity in faecal content, although it remained similar in ileum (figure 7E). Changes were also observed in other bacterial genera with an increase in *AF12*, *Parracoccus*, *Acinobacter* and a decrease in *Clostridium*, *Coprobacillus* and *Streptococcus* (online supplemental figure 6A). Of note, macrophages, which are able to produce TNF α in the LP, were not affected by anti-TNF α treatment (online supplemental figure 6B). We next analysed dendritic cells (DCs) since we had previously shown that loss of gut integrity in NOD mice could lead to bacterial components translocation and increased CD11c⁺CD11b⁺CD103⁺ DCs frequencies and activation.²⁴ Indeed, anti-TNF α antibodies induced a significant reduction of this DCs subset in ileum of BDC2.5 T cell-transferred mice, however, such reduction was not observed in PLN (figure 7F and online supplemental figure 6C). Moreover, anti-TNF α treatment also decreased ileum CD11c⁺CD11b⁺CD103⁺ DCs activation as shown by their lower surface levels of MHC-II compared with non-treated control mice (figure 7F). Interestingly, anti-TNF α reduced the frequency and absolute numbers of BDC2.5 T cells in ileum but not in PLN (figure 7G). This was associated with a significant increase of FOXP3⁺ BDC2.5 T cell frequency in ileum and not in PLN (figure 7H and online supplemental figure 6D). Further analysis of autoreactive T cells showed a significant reduction of their IFN- γ production in both ileum and PLN from mice treated with anti-TNF α compared with control mice whereas TNF α production by BDC2.5 T cells remained unchanged (figure 7I and online supplemental figure 6E). Finally, the decreased IFN- γ production by BDC2.5 T cells in anti-TNF α treated mice was associated with a lower incidence of T1D and less severe insulinitis (figure 7J). Altogether these data support again a key role for gut inflammation in promoting anti-islet T cell effector function leading to pancreatic infiltration and T1D onset. Reducing inflammation (by anti-TNF α treatment) helps correcting T1D-associated SFB dysbiosis and mucosal dysfunctions (online supplemental figure 7).

DISCUSSION

Our study brings new knowledge on the nature and the origin of gut mucosa and microbiota alterations associated with T1D development. Using several mouse models of T1D, we showed that with disease development (1) gut immune cells produced lower levels of IL-17A, IL-22 and IL-23A, (2) intestinal ECs displayed decreased expression markers of gut integrity (Claudin 4, Occludin, Tight junction protein 1 and Mucin 2), and decreased fucosylation levels and (3) gut microbiota changes were associated with reduced abundance of SFB in ileum. Moreover, our results revealed that these modifications were not observed on metabolic induction of hyperglycaemia. Several reports had described gut alterations in T1D, obesity and T2D as well as after induction of hyperglycaemia by insulin receptor blockade.^{12 13 41} While NOD mice develop gut alterations in several weeks, the other diabetes models (STZ multi-low-dose injections, S961-treatment and BDC2.5 T cell transfer) induced diabetes within a week. Therefore, chronicity of gut inflammation is not required for gut alterations observed in T1D. Modifications of gut microbiota composition were very similar between spontaneously diabetic NOD, and BDC2.5 T cells transferred *Trac*^{-/-} recipient mice in contrast to gut microbiota modification

observed in metabolically induced hyperglycaemic mice. Taken together, this suggests that targeting only hyperglycaemia in T1D would not resolve mucosal dysfunctions whereas treating inflammation could restore intestinal homeostasis.

T1D is characterised by the development of autoimmune responses associated with inappropriate activation of immune cells that infiltrate the pancreas.¹⁻³ We and others have described gut inflammation associated with T1D suggesting that gut inflammation could lead to decreased mucosal IL-17A, IL-22 and IL-23A production, EC defect and loss of ileum SFB.^{24 42} It was striking that BDC2.5 T cell frequency was higher in the gut mucosa than in MLN and PLN, and they produced the highest level of TNF α in the gut. TNF α production by low-proliferating BDC2.5 T cells in ileum is probably due to the proinflammatory environment rather than potential microbiota cross-reactivity. These results prompted us to assess the efficiency of anti-TNF α treatment, which is a common treatment in Crohn's disease.⁴³ This treatment had a major effect on the gut mucosa as it increased IL-22 and IL-17A production, fucosylation of ECs and SFB abundance. Moreover, lower DC activation and increased T regulatory cell frequency were observed in the ileum but not in PLN supporting a primary effect on the gut mucosa. Furthermore, it has been reported that gut IL-10⁺ T regulatory cells could migrate to PLN.⁴⁴ Systemic anti-TNF α treatment does not exclude that anti-inflammatory mAb could directly act on pathogenic cells in PLN and pancreas. TNF α can exert an ambivalent role in the development of T1D in mouse models⁴⁵⁻⁴⁸ and a previous report has shown that anti-TNF α treatment at the perinatal period in NOD mice prevents T1D onset.⁴⁷ Of note, gut mucosa was not analysed in this pioneer study. Interestingly, anti-TNF α treatment in a patient with Crohn's disease and T1D not only improved intestinal pathology but also T1D.⁴⁹ Our present data further highlights the relevance of controlling gut inflammatory status to dampen pathogenic anti-islet T cells in PLN, severe insulinitis and T1D.

We showed for the first time that SFB levels in ileum and faeces were decreased during the establishment of spontaneous diabetes in NOD mice, in T1D induced by STZ treatment in NOD and C57BL/6J mice as well as on transfer of autoreactive BDC2.5 T cells. In contrast, metabolic induction of hyperglycaemia enhanced SFB levels in ileum and faeces and is reminiscent with SFB requiring high glucose levels to grow on ECs.⁵⁰ Thus, low SFB level in T1D might be a consequence of local inflammation, despite increased glycaemia. This finding is interesting in light to previous studies asking whether SFB could exert a protective role against T1D. Comparison of two NOD colonies from different breeding companies showed that the colony harbouring SFB had a lower incidence of T1D than the other colony.⁴² In another study, germ-free NOD mice were colonised with SFB, however, incidence of T1D was only slightly decreased in recipient males, not females.⁵¹ Our study established a strong parallel between SFB abundance in ileum and intestinal IL-17A and IL-22 production. Both cytokines can be induced by SFB³²⁻³⁶ and maintain gut homeostasis thereby preventing bacterial component translocation and inflammation. Several mechanisms could be at play. IL-22 can upregulate *Fut2* expression and ECs fucosylation favouring the maintenance of commensal flora.^{29 30} IL-22 can also maintain gut integrity by promoting expression of tight junctions proteins and production of mucus preventing pathogenic bacteria invasiveness.⁵² IL-22 could also alleviate pancreatic β cell stress, preventing the generation of islet neoantigens playing a critical role in the autoimmune attack of β cells.⁵²⁻⁵⁴

The role of SFB in the dampening of gut mucosa inflammation and diabetes development can also be associated with increased

diabetes incidence after antibiotic treatment.⁵⁵ Indeed, SFB is extremely sensitive to antibiotics.⁵⁶ Another protective role of SFB could be related to their ability to prevent bacterial and viral infections. SFB can induce the production of IL-22 that controls *Citrobacter rodentium* infection,⁵⁷ an intestinal pathogenic bacteria that is known to accelerate T1D development in NOD mice.⁸ Similarly, SFB prevents rotavirus infection in mice that might be involved in T1D development.^{56,58} Thus, our study provides new insights in the deleterious role of gut inflammation against protective commensal microbiota in the physiopathology of T1D.

MATERIALS AND METHODS

Mice

Male and female C57BL/6J, male and female NOD, female ROR γ -GFP NOD, female BDC2.5 CD45.2^{+/+} *Trac*^{-/-} NOD and female recipient CD45.1^{+/+} *Trac*^{-/-} NOD mice were previously described.^{24,59} All mice were bred under specific pathogen-free conditions. Detailed experimental methods concerning the different mice models are described in online supplemental methods.

Cell preparations and flow cytometry

Cells were prepared from different tissues and analysed by flow cytometry as described in online supplemental methods.

Isolation of DNA, RNA and RT

For DNA extraction, fresh stool or small pieces of ileum tissue were weighted, recovered, immediately frozen in liquid nitrogen on collection, and stored at -80°C until DNA isolation. DNA extraction was performed using NucleoSpin Tissue (Macherey-Nagel) following the manufacturer's instructions. Sections of liver near the portal vein were recovered from mice at different ages and DNA was extracted as previously described.²⁴ For RNA isolation, cells were lysed in RLT buffer with 1% β -mercaptoethanol, and mRNA was purified from lysed cells using RNeasy Mini Kit (Qiagen). cDNA was synthesised using the Superscript III reverse transcriptase (Invitrogen). Quantitative PCR analysis was performed with SYBR Green (Roche) and analysed using a LightCycler 480 (Roche). The relative expression was calculated using the $2^{-\Delta\Delta\text{Ct}}$ method and normalised to the expression of the housekeeping gene *Gapdh* or the expression of total bacteria, as appropriate. The stability of *Gapdh* expression was confirmed by comparison with hypoxanthine phosphoribosyl-transferase mRNA expression. Used primers and their sequences are described as follows (online supplemental table 2).

In vivo analysis of intestinal permeability

Intestinal permeability was determined by measuring the level of FITC dextran as described in online supplemental methods.

Bacterial dissemination and identification

Liver was collected at different time points in aseptic conditions. Tissues were processed to harvest cells, then lysed and plated to identify bacteria by mass spectrometry as described in online supplemental methods.

Fecal microbiota analysis

16S rRNA gene amplification and library constructions were performed according to Illumina recommendations. Sequencing was performed on an Illumina MiSeq. Taxonomy and data analyses were conducted using Quantitative Insights Into Microbial Ecology (QIIME). The detailed procedures of mice faecal

microbiota 16S sequencing are described in online supplemental methods.

Statistical analysis

Statistical analyses were performed with Prism software (Graph Pad V8.3). All datasets were tested for normal distribution using the Shapiro-Wilk normality test. Datasets were compared using either parametric two-tailed unpaired t-test, non-parametric two-tailed Mann-Whitney or Kruskal-Wallis tests with multiple comparisons Dunn's post-test, as appropriate. Significant differences in taxonomic abundances were assessed with non-parametric Kruskal-Wallis test with the false-discovery rate correction implemented in QIIME. Diabetes incidence was plotted according to the Kaplan-Meier method and statistical differences were analysed using the Mantel-Cox (log-rank test). Differences were considered significant at $p < 0.05$ (* $p < 0.05$, ** $p < 0.01$, *** $p < 0.001$, **** $p < 0.0001$).

Author affiliations

¹Université de Paris, Institut Cochin, INSERM U1016, CNRS UMR 8104, Paris, France

²Laboratoire d'Excellence Inflamex, Université de Paris, Paris, France

³Institut Pasteur, INSERM U1202, Paris, France

⁴Department of Biomedical Sciences - IRCCS, Via Rita Levi Montalcini, 20090 Pieve Emanuele, Humanitas University, Milan, Italy

⁵IRCCS, Via Manzoni 56, 20089 Rozzano, Humanitas Clinical and Research Center, Milan, Italy

⁶Université de Toulouse, Institut de Recherche en Santé Digestive, INSERM U1220, INRAE, ENVT, Toulouse, France

Acknowledgements We thank CYBIO, GENOM'IC and HistIM facilities platform of the Cochin Institute. We thank Marcio Do Cruzeiro, Nadia Boussetta, Matthieu Benard from the mouse facility platform of Cochin Institute as well as Claire Lacoste, Nicoleta Mitrea, Georgeta Fagie and Soizic Jezequel from UMS 028 mouse facility platform of Charles Foix Hospital. We thank Julia Adelöf, Ivo Notario, Jennifer Da Silva, and Sandrine Olivre for technical help. We thank Yannick Allanoire for providing Infliximab. We thank Alexandra Corbett, Jamie Rossjohn and James McCluskey for providing mouse MR1 tetramers. We thank Michel Samson for providing IL23a PCR primers. We thank Amine Toubal, Valérie Gaboriau-Routhiau and Nadine Cerf-Bensussan for critical reading of the manuscript. We also thank Servier Medical Art for the free medical images, licensed under the Creative Commons Attribution 3.0 Unported License.

Contributors MR, LBea, OR and LBer performed most of the experiments and data analysis; LC performed experiments and data analysis; AS and TP produced 16S sequencing as well as bioinformatics analyses; DG and LR participated in the S961 experiments; JM and AT contributed to CFU analyses; NV provided Infliximab; SG, A-FB, MR, NV and PS provided intellectual input. MR, LBea, LBer, UCR and AL wrote the paper. AL supervised the whole project.

Funding This work was supported by Agence Nationale de la Recherche (ANR-11-IDEX-0005-02 Laboratory of Excellence INFLAMEX and ANR-17-CE14-0002-01 Diab1MAIT), Fondation pour la Recherche Médicale (DEQ20140329520 and EQU201903007779), the INSERM crosscutting program on microbiota and the European Foundation for the Study of Diabetes–Juvenile Diabetes Research Foundation–MR, OR and LBer were supported by the French Ministry of Research.

Competing interests None declared.

Patient consent for publication Not required.

Ethics approval This study was approved by the Ethics Committee on Animal Experimentation (APAFIS#3474–2015102016444419 v3 and APAFIS#17 515–201811091441828 V4).

Provenance and peer review Not commissioned; externally peer reviewed.

Data availability statement Data are available on reasonable request at the corresponding author (agnes.lehuen@inserm.fr)

Supplemental material This content has been supplied by the author(s). It has not been vetted by BMJ Publishing Group Limited (BMJ) and may not have been peer-reviewed. Any opinions or recommendations discussed are solely those of the author(s) and are not endorsed by BMJ. BMJ disclaims all liability and responsibility arising from any reliance placed on the content. Where the content includes any translated material, BMJ does not warrant the accuracy and reliability of the translations (including but not limited to local regulations, clinical guidelines, terminology, drug names and drug dosages), and is not responsible for any error and/or omissions arising from translation and adaptation or otherwise.

ORCID iDs

Matthieu Rouland <http://orcid.org/0000-0002-8019-7629>Léo Bertrand <http://orcid.org/0000-0001-5584-3476>Latif Rachdi <http://orcid.org/0000-0002-1089-2837>Agnès Lehen <http://orcid.org/0000-0002-0450-3321>

REFERENCES

- Atkinson MA, Eisenbarth GS, Michels AW. Type 1 diabetes. *Lancet* 2014;383:69–82.
- Lehen A, Diana J, Zaccane P, et al. Immune cell crosstalk in type 1 diabetes. *Nat Rev Immunol* 2010;10:501–13.
- Diana J, Simoni Y, Furio L, et al. Crosstalk between neutrophils, B-1a cells and plasmacytoid dendritic cells initiates autoimmune diabetes. *Nat Med* 2013;19:65–73.
- Meddings JB, Jarand J, Urbanski SJ, et al. Increased gastrointestinal permeability is an early lesion in the spontaneously diabetic BB rat. *Am J Physiol* 1999;276:G951–7.
- Alam C, Valkonen S, Palagani V, et al. Inflammatory tendencies and overproduction of IL-17 in the colon of young NOD mice are counteracted with diet change. *Diabetes* 2010;59:2237–46.
- Sapone A, de Magistris L, Pietzak M, et al. Zonulin upregulation is associated with increased gut permeability in subjects with type 1 diabetes and their relatives. *Diabetes* 2006;55:1443–9.
- Graham S, Courtois P, Malaisse WJ, et al. Enteropathy precedes type 1 diabetes in the BB rat. *Gut* 2004;53:1437–44.
- Lee AS, Gibson DL, Zhang Y, et al. Gut barrier disruption by an enteric bacterial pathogen accelerates insulinitis in NOD mice. *Diabetologia* 2010;53:741–8.
- Miranda MCG, Oliveira RP, Torres L, et al. Frontline science: abnormalities in the gut mucosa of non-obese diabetic mice precede the onset of type 1 diabetes. *J Leukoc Biol* 2019;106:513–29.
- Carratù R, Seconduolo M, de Magistris L, et al. Altered intestinal permeability to mannitol in diabetes mellitus type 1. *J Pediatr Gastroenterol Nutr* 1999;28:264–9.
- Kuitunen M, Saukkonen T, Ilonen J, et al. Intestinal permeability to mannitol and lactulose in children with type 1 diabetes with the HLA-DQB1*02 allele. *Autoimmunity* 2002;35:365–8.
- Vaarala O. Leaking gut in type 1 diabetes. *Curr Opin Gastroenterol* 2008;24:701–6.
- Thaiss CA, Levy M, Grosheva I, et al. Hyperglycemia drives intestinal barrier dysfunction and risk for enteric infection. *Science* 2018;359:1376–83.
- Hansen CHF, Krych L, Buschard K, et al. A maternal gluten-free diet reduces inflammation and diabetes incidence in the offspring of NOD mice. *Diabetes* 2014;63:2821–32.
- Dunne JL, Triplett EW, Gevers D, et al. The intestinal microbiome in type 1 diabetes. *Clin Exp Immunol* 2014;177:30–7.
- Kostic AD, Gevers D, Siljander H, et al. The dynamics of the human infant gut microbiome in development and in progression toward type 1 diabetes. *Cell Host Microbe* 2015;17:260–73.
- Alkanani AK, Hara N, Gottlieb PA, et al. Alterations in intestinal microbiota correlate with susceptibility to type 1 diabetes. *Diabetes* 2015;64:3510–20.
- Westerholm-Ormio M, Vaarala O, Pihkala P, et al. Immunologic activity in the small intestinal mucosa of pediatric patients with type 1 diabetes. *Diabetes* 2003;52:2287–95.
- Pellegrini S, Sordi V, Bolla AM, et al. Duodenal mucosa of patients with type 1 diabetes shows distinctive inflammatory profile and microbiota. *J Clin Endocrinol Metab* 2017;102:1468–77.
- Hardin JA, Donegan L, Woodman RC, et al. Mucosal inflammation in a genetic model of spontaneous type 1 diabetes mellitus. *Can J Physiol Pharmacol* 2002;80:1064–70.
- Leeds JS, Hopper AD, Hadjivassiliou M, et al. Inflammatory bowel disease is more common in type 1 diabetes mellitus. *Gut* 2011;60:A208.
- Rewers M, Eisenbarth GS. Celiac disease in T1DM—the need to look long term. *Nat Rev Endocrinol* 2011;8:5–8.
- Badami E, Sorini C, Coccia M, et al. Defective differentiation of regulatory Foxp3+ T cells by small-intestinal dendritic cells in patients with type 1 diabetes. *Diabetes* 2011;60:2120–4.
- Rouxel O, Da Silva J, Beaudoin L, et al. Cytotoxic and regulatory roles of mucosal-associated invariant T cells in type 1 diabetes. *Nat Immunol* 2017;18:1321–31.
- Colonna M. Interleukin-22-producing natural killer cells and lymphoid tissue inducer-like cells in mucosal immunity. *Immunity* 2009;31:15–23.
- Lee JS, Tato CM, Joyce-Shaikh B, et al. Interleukin-23-Independent IL-17 production regulates intestinal epithelial permeability. *Immunity* 2015;43:727–38.
- Dudakov JA, Hanash AM, van den Brink MRM. Interleukin-22: immunobiology and pathology. *Annu Rev Immunol* 2015;33:747–85.
- Ivanov II, McKenzie BS, Zhou L, et al. The orphan nuclear receptor ROR γ mat directs the differentiation program of proinflammatory IL-17+ T helper cells. *Cell* 2006;126:1121–33.
- Pickard JM, Maurice CF, Kinnebrew MA, et al. Rapid fucosylation of intestinal epithelium sustains host-commensal symbiosis in sickness. *Nature* 2014;514:638–41.
- Goto Y, Obata T, Kunisawa J, et al. Innate lymphoid cells regulate intestinal epithelial cell glycosylation. *Science* 2014;345:1254009.
- Chase DG, Erlandsen SL. Evidence for a complex life cycle and endospore formation in the attached, filamentous, segmented bacterium from murine ileum. *J Bacteriol* 1976;127:572–83.
- Ivanov II, Atarashi K, Manel N, et al. Induction of intestinal Th17 cells by segmented filamentous bacteria. *Cell* 2009;139:485–98.
- Gaboriau-Routhiau V, Rakotobe S, Lécuyer E, et al. The key role of segmented filamentous bacteria in the coordinated maturation of gut helper T cell responses. *Immunity* 2009;31:677–89.
- Goto Y, Panea C, Nakato G, et al. Segmented filamentous bacteria antigens presented by intestinal dendritic cells drive mucosal Th17 cell differentiation. *Immunity* 2014;40:594–607.
- Lécuyer E, Rakotobe S, Lengliné-Garnier H, et al. Segmented filamentous bacterium uses secondary and tertiary lymphoid tissues to induce gut IgA and specific T helper 17 cell responses. *Immunity* 2014;40:608–20.
- Omenetti S, Bussi C, Metidji A, et al. The intestine harbors functionally distinct homeostatic tissue-resident and inflammatory Th17 cells. *Immunity* 2019;51:77–89.
- Leiter EH. Multiple low-dose streptozotocin-induced hyperglycemia and insulinitis in C57BL mice: influence of inbred background, sex, and thymus. *Proc Natl Acad Sci U S A* 1982;79:630–4.
- Schäffer L, Brand CL, Hansen BF, et al. A novel high-affinity peptide antagonist to the insulin receptor. *Biochem Biophys Res Commun* 2008;376:380–3.
- Beaudoin L, Diana J, Ghazarian L, et al. Plasmacytoid dendritic cells license regulatory T cells, upon iNKT-cell stimulation, to prevent autoimmune diabetes. *Eur J Immunol* 2014;44:1454–66.
- Hu Y, Peng J, Li F, et al. Evaluation of different mucosal microbiota leads to gut Microbiota-Based prediction of type 1 diabetes in NOD mice. *Sci Rep* 2018;8:15451.
- Winer DA, Winer S, Dranse HJ, et al. Immunologic impact of the intestine in metabolic disease. *J Clin Invest* 2017;127:33–42.
- Kriegel MA, Sefik E, Hill JA, et al. Naturally transmitted segmented filamentous bacteria segregate with diabetes protection in nonobese diabetic mice. *Proc Natl Acad Sci U S A* 2011;108:11548–53.
- Colombel JF, Sandborn WJ, Reinisch W, et al. Infliximab, azathioprine, or combination therapy for Crohn's disease. *N Engl J Med* 2010;362:1383–95.
- Yu H, Gagliani N, Ishigame H, et al. Intestinal type 1 regulatory T cells migrate to periphery to suppress diabetogenic T cells and prevent diabetes development. *Proc Natl Acad Sci U S A* 2017;114:10443–8.
- Jacob CO, Aiso S, Michie SA, et al. Prevention of diabetes in nonobese diabetic mice by tumor necrosis factor (TNF): similarities between TNF-alpha and interleukin 1. *Proc Natl Acad Sci U S A* 1990;87:968–72.
- Jacob CO, Aiso S, Schreiber RD, et al. Monoclonal anti-tumor necrosis factor antibody renders non-obese diabetic mice hypersensitive to irradiation and enhances insulinitis development. *Int Immunol* 1992;4:611–4.
- Yang XD, Tisch R, Singer SM, et al. Effect of tumor necrosis factor alpha on insulin-dependent diabetes mellitus in NOD mice. I. the early development of autoimmunity and the diabetogenic process. *J Exp Med* 1994;180:995–1004.
- Green EA, Gorelik L, McGregor CM, et al. Cd4+ Cd25+ T regulatory cells control anti-islet CD8+ T cells through TGF-beta-TGF-beta receptor interactions in type 1 diabetes. *Proc Natl Acad Sci U S A* 2003;100:10878–83.
- Timper K, Hruz P, Beglinger C, et al. Infliximab in the treatment of Crohn disease and type 1 diabetes. *Diabetes Care* 2013;36:e90–1.
- Schnupf P, Gaboriau-Routhiau V, Gros M, et al. Growth and host interaction of mouse segmented filamentous bacteria in vitro. *Nature* 2015;520:99–103.
- Yurkovetskiy L, Burrows M, Khan AA, et al. Gender bias in autoimmunity is influenced by microbiota. *Immunity* 2013;39:400–12.
- Rutz S, Wang X, Ouyang W. The IL-20 subfamily of cytokines—from host defence to tissue homeostasis. *Nat Rev Immunol* 2014;14:783–95.
- Hasnain SZ, Borg DJ, Harcourt BE, et al. Glycemic control in diabetes is restored by therapeutic manipulation of cytokines that regulate beta cell stress. *Nat Med* 2014;20:1417–26.
- Delong T, Wiles TA, Baker RL, et al. Pathogenic CD4 T cells in type 1 diabetes recognize epitopes formed by peptide fusion. *Science* 2016;351:711–4.
- Livanos AE, Greiner TU, Vangay P, et al. Antibiotic-Mediated gut microbiome perturbation accelerates development of type 1 diabetes in mice. *Nat Microbiol* 2016;1:16140.
- Shi Z, Zou J, Zhang Z, et al. Segmented filamentous bacteria prevent and cure rotavirus infection. *Cell* 2019;179:644–58.
- Zheng Y, Valdez PA, Danilenko DM, et al. Interleukin-22 mediates early host defense against attaching and effacing bacterial pathogens. *Nat Med* 2008;14:282–9.
- Honeyman MC, Coulson BS, Stone NL, et al. Association between rotavirus infection and pancreatic islet autoimmunity in children at risk of developing type 1 diabetes. *Diabetes* 2000;49:1319–24.
- Katz JD, Benoist C, Mathis D. T helper cell subsets in insulin-dependent diabetes. *Science* 1995;268:1185–8.

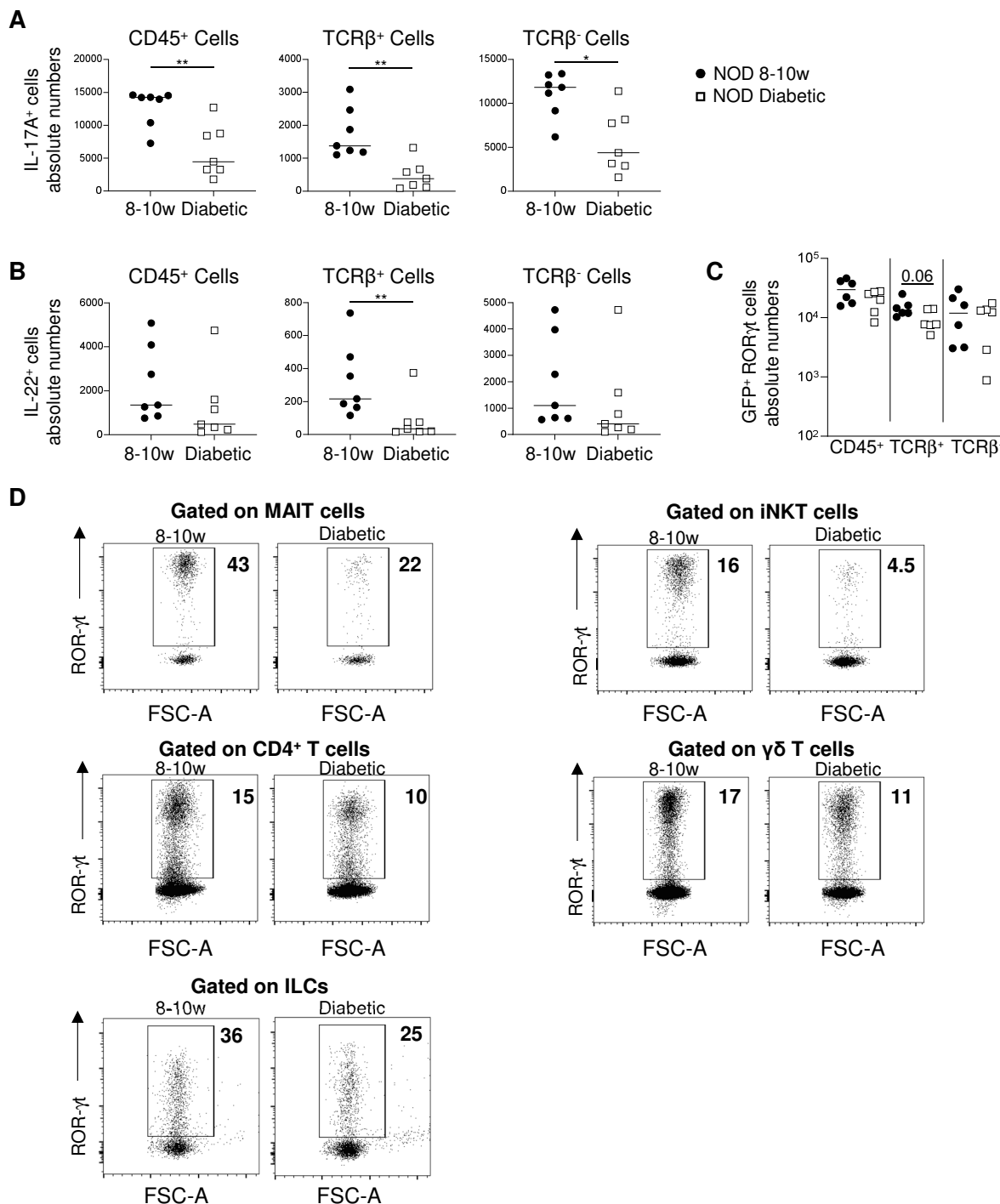


Figure S1. Analysis of IL-17, IL-22 and RORγt-GFP⁺ expression in LP cells of 8-10w and diabetic NOD mice. Lamina propria (LP) cells from small intestine of prediabetic (8-10 weeks) and diabetic females NOD mice were analyzed by flow cytometry. (A, B) Mice were stimulated for 2 hours *in vivo* by injection of flagellin. Absolute numbers of IL-17A⁺ cells (A) or IL-22⁺ (B) cells CD45⁺, TCRβ⁺ or TCRβ⁻ lymphoid cells (n=7 mice per group). (C) Absolute numbers of RORγt-GFP⁺ cells among CD45⁺, TCRβ⁺ or TCRβ⁻ lymphoid cells (n=6 mice per group). (D) Representative dot-plots and percentages of RORγt-GFP⁺ among MAIT, iNKT, CD4⁺ T, TCRγδ⁺ cells and ILCs in LP according to cell size (FSC-A).

SUPPLEMENTARY MATERIAL

Supplementary methods

Diabetes diagnostic. Mice were tested either weekly, or daily after STZ, S961 treatment and cell transfer experiments, and considered diabetic after two consecutive positive urine glucose tests (DIABUR-TEST 5000, Roche), confirmed by glycemia > 200 mg/dL (ACCU-CHEK, Roche). All diabetic mice used were recent onset (< 3 days after diagnostic).

Streptozotocin (STZ) diabetes induction. To induce hyperglycemia, STZ (Sigma-Aldrich) was diluted in sodium citrate buffer (pH 4.5), just before use. Male NOD and C57BL/6J mice at 8 to 12 weeks of age were injected *i.p.* daily for three consecutive days with 50mg.kg⁻¹ of STZ. Control mice were injected with citrate buffer.

Insulin receptor antagonist treatment. For continuous insulin receptor antagonist (S961; gift from Dr. Lauge Schäffer, Novo Nordisk) administration [1], ALZET® mini osmotic pumps (model 2001) were implanted subcutaneously in the back of the mice and maintained for 7 days. S961 (20nmol/week) was delivered at 0.5 μ L.hour⁻¹. Control mice were implanted with pumps containing PBS.

Transfer experiment. CD4⁺ CD62L⁺ BDC2.5 T cells were obtained from female BDC2.5 CD45.2^{+/+} *Trac*^{-/-} NOD mice. CD4⁺ BDC2.5 T cells were negatively selected from total splenocytes (Dynal beads) then FACS sorted on a BD Biosciences FACSaria III sorter as CD4⁺ CD62L⁺. These cells were injected *i.v.* (0.3 to 0.5 $\times 10^6$ cells/mouse) into 6 to 8-week-old female recipient CD45.1^{+/+} *Trac*^{-/-} NOD to induce diabetes or in 13-week-old NOD mice to follow BDC2.5 proliferation in mice already pre-diabetic.

Anti-TNF α treatment. *Trac*^{-/-} NOD mice transferred with CD4⁺ BDC2.5 T cells were injected *i.p.* on day 0, 3, and 6 after transfer with 10mg/kg of human Infliximab anti-TNF α treatment

(Remicade®). As antibody control, mice were injected with 10mg/kg of InVivoPlus human IgG1 isotype control (Bio X Cell).

Cell preparations. Cells were prepared from different tissues as described below. For intestine cell isolation, mice were sacrificed and the small intestine (ileum part) was removed from the mice, cleared from feces, fat tissue, and Peyer's patches using HBSS without Ca^{2+} and Mg^{2+} containing 10 mM HEPES solution. Miltenyi Lamina Propria Dissociation Kit for mouse was used to prepare epithelial and *lamina propria* cells. After passage through a 100 μm filter, the cell suspension was subjected to Percoll (GE Healthcare) density gradient of 40% and 80%, and the interface between the layers containing intraepithelial lymphocytes or *lamina propria* lymphocytes were collected and suspended in PBS containing 2% FCS and 0.1% sodium azide. For the preparation of mouse DC from lymph nodes, mice were sacrificed, organs were cut in small pieces and digested at 37°C for 30 min with 2 mL of collagenase D (1.0 $\text{mg}\cdot\text{mL}^{-1}$, Roche) solution. Digestion was stopped by adding a large volume of cold Roswell Park Medium Intermediate (RPMI) medium supplemented with 5% FCS, and cells were washed and filtered on cell strainers (40 μm , BD Falcon) before labeling. For islets cells isolations, pancreas were perfused with 3 mL of a collagenase P solution (1.5 $\text{mg}\cdot\text{mL}^{-1}$, Roche), and islets were isolated as previously described [2].

Flow cytometry. Labeling was performed in PBS containing 2% FCS and 0.1% sodium azide. Antibodies, lectin, and tetramers are listed below. Data acquisition was performed using a BD Biosciences LSR Fortessa or FACS-ARIA III cytometer. Flow cytometric analyses were performed with the FlowJo analysis software V10.6 (Tree Star).

Intracellular labeling. For cytokine labeling, cells were stimulated in RPMI supplemented with 10% FCS, with PMA (10 ng/mL) and ionomycin (1 $\mu\text{g/mL}$) in the presence of Brefeldin A (10 $\mu\text{g/mL}$) for 4 h at 37°C (all reagents from Sigma-Aldrich) or cells were stimulated in vivo by *i.v.* injection of flagellin (FLA-PA) at 3 $\mu\text{g}/\text{mouse}$ 2 h before analysis. After surface

labeling, cells were fixed and permeabilized with Cytofix/Cytoperm kit (BD Biosciences) as previously described. For Ki-67 nuclear cell proliferation and Foxp3/Transcription factor staining, after surface staining, cells were fixed and permeabilized with Foxp3/Transcription Factor staining buffer set (eBioscience 00-5523) as previously described [3].

Antibodies, lectin, and tetramers. TCR β (H57), TCR $\gamma\delta$ (GL3), CD45 (30F11), CD8 α (53-6.7), CD103 (M290), I-Ak (10-3.6), CD62L (ML-14), CD86 (GL1), CD90.1 (HIS-51), Ki-67 (B56), IL-17A (TC11-18H10), TNF α (MP6-XTT22) and IFN- γ (XMG1.2) mAbs, were from BD Biosciences; CD19 (6D5), CD4 (GK1.5), CD11b (M1/70), CD127 (A7R34) and IL-22 (5164) mAbs, were from Biolegend; CD11c (N418), CD326 (G8.8), FOXP3 (FJK-16s) and F4/80 (BM8) mAbs were from eBioscience; UEA-1 was from Vector. The alpha-galactosylceramide-CD1d tetramer was prepared in house and coupled to streptavidin-BV421 (Biolegend). Biotinylated mouse MR1 tetramers loaded with the active ligand (5-OP-RU) were used to specifically identify MAIT cells. Cells were stained with CD1d or MR1 tetramers for 45 min at RT before surface staining with mAbs.

***In vivo* analysis of intestinal permeability.** Briefly, mice were water-starved 4 hours prior to gavage with FITC-dextran (4 kDa; Sigma, 44 mg/100 g body weight). 150 μ L of blood was collected 4 h later and centrifuged at 3000 g for 20 min at 4°C. Plasma (50 μ L) was diluted volume to volume with PBS to determine fluorescence using a SPARK 10M multimode microplate reader (TECAN). The concentration was determined using FITC-dextran serial dilutions.

Bacterial dissemination and identification. Liver was collected at different time points in aseptic conditions. Tissues were collected in 1X PBS containing gentamycin (50 μ g/mL) and incubated 30 min at 37°C. Then they were digested with collagenase D (1 mg/mL) for 30 min at 37°C. Dissociated cell suspensions were obtained and number and viability of cells determined using trypan blue exclusion test. 10⁷ cells were then lysed with 0.5% sodium-

deoxycholate and plated on terrific broth agar plates without antibiotics to evaluate bacterial dissemination after 24 or 48 hours at 37°C, under both aerobic and anaerobic conditions, respectively. CFU were enumerated and normalized to the number of plated cells. Mass spectrometry MALDI-TOF (matrix-assisted laser desorption–ionization time of flight) (Bruker) was used to identify bacterial species according to the manufacturer’s recommendations.

16S rRNA amplification and sequencing. 16S rRNA gene amplification and library constructions were performed according to Illumina recommendations. A first PCR round was performed using 12.5 ng of DNA using primers targeting the 16S rRNA gene V3 and V4 regions and as follows: forward primer 341F 5’-*TCGTCGGCAGCGTCAGATGTGTATAAGAGACAGCCTACGGGNGGCWGCAG*-3’ and reverse primer 805R 5’-*GTCTCGTGGGCTCGGAGATGTGTATAAGAGACAGGACTACHVGGGTATCTAATCC*-3’, where the Illumina adapters are indicated in italics. After 25 cycles, PCR products were purified using AMPure XP beads (Beckman Coulter Genomics) according to the manufacturer’s recommendations. A second PCR was performed to attach dual indices using the Nextera XT Index kit (Illumina). After eight cycles, PCR products were purified using AMPure XP beads (Beckman Coulter Genomics). PCR were also performed using extraction buffer alone (DNA extraction negative controls) or water as template and used as controls for 16S rRNA gene sequencing analysis. The size of the libraries (~600 bp) and their quantification were determined by Fragment Analyzer (Advanced Analytical) using the High Sensitivity NGS Fragment Analysis kit. Purified amplicons were pooled in equimolar concentration to obtain a 6 pM library containing 10% of PhiX control. Sequencing was performed on an Illumina MiSeq instrument using the paired-end 300 base pairs protocol.

Sequence analysis. After sequencing of 141 samples, including 4 water samples used as template controls (water), a total of 30,310,223 read pairs were yielded (mean 221,242 read

pairs per sample with a median of 188,982). The demultiplexed read pairs were first assembled using FLASH v1.2.11 [4]. The FLASH software was run with error-correction feature to find and correct all ambiguous base pairs in the region where both reads overlap (average size of the overlapping region was 120 bp). Primer sequences and any fragments containing ambiguous bases N or shorter than 400 were removed (cutadapt 2.6 and PRINSEQ-lite 0.20.3) [5,6]. A mean Phred quality score of 28 was required to keep fragments for downstream analysis. Taxonomy and data analyses were conducted using QIIME (v1.9.1) [7] following these steps: (i) `pick_otu.py` takes advantage of the UCLUST algorithm to cluster sequences into operational taxonomic units (OTUs) using 97% similarity [8]; (ii) `pick_rep_set.py` to obtain a representatives set of OTUs, including a representative sequence, corresponding to the centroid of the associated cluster; for each OTU (iii) `assign_taxonomy.py` to apply taxonomy assignment for the all sequences of the representative set, exploiting the Uclust algorithm (using default parameters) and both Greengenes 13.8 16S rRNA genes sequence and human intestinal 16S rRNA gene taxonomic (HitDB) databases [9,10]. To build the phylogenic tree of OTU representative sets, the multiple-alignment step was performed with PyNAST based on a similarity of 75% [11]. The phylogenic tree was created using `make_phylogeny.py` with `tree_method_default` parameter based on the FastTree algorithm [12]. The generated phylogenic tree was used to calculate core diversity metrics; β -diversity [based on weighted/unweighted unifracs metrics] [13], and α -diversity was calculated for different depth of rarefactions. The PCoA plot and β -diversity, generated by Qiime using unweighted unifracs metrics, confirm the intergroup similarity and intra group low similarity of microbiota [7,13]. The set of OTUs that are observed in a given fraction of samples was defined as Core OTU and was calculated using `compute_core_microbiom.py` with a fraction of 50% of total OTUs.

Supplementary references

- 1 Schäffer L, Brand CL, Hansen BF, *et al.* A novel high-affinity peptide antagonist to the insulin receptor. *Biochem Biophys Res Commun* 2008;**376**:380–3. doi:10.1016/j.bbrc.2008.08.151
- 2 Beaudoin L, Diana J, Ghazarian L, *et al.* Plasmacytoid dendritic cells license regulatory T cells, upon iNKT-cell stimulation, to prevent autoimmune diabetes. *Eur J Immunol* 2014;**44**:1454–66. doi:10.1002/eji.201343910
- 3 Rouxel O, Da Silva J, Beaudoin L, *et al.* Cytotoxic and regulatory roles of mucosal-associated invariant T cells in type 1 diabetes. *Nat Immunol* 2017;**18**:1321–31. doi:10.1038/ni.3854
- 4 Magoč T, Salzberg SL. FLASH: fast length adjustment of short reads to improve genome assemblies. *Bioinforma Oxf Engl* 2011;**27**:2957–63. doi:10.1093/bioinformatics/btr507
- 5 Martin M. Cutadapt removes adapter sequences from high-throughput sequencing reads. *EMBnet.journal* 2011;**17**:10–2. doi:10.14806/ej.17.1.200
- 6 Schmieder R, Edwards R. Quality control and preprocessing of metagenomic datasets. *Bioinforma Oxf Engl* 2011;**27**:863–4. doi:10.1093/bioinformatics/btr026
- 7 Caporaso JG, Kuczynski J, Stombaugh J, *et al.* QIIME allows analysis of high-throughput community sequencing data. *Nat Methods* 2010;**7**:335–6. doi:10.1038/nmeth.f.303
- 8 Edgar RC. Search and clustering orders of magnitude faster than BLAST. *Bioinforma Oxf Engl* 2010;**26**:2460–1. doi:10.1093/bioinformatics/btq461
- 9 DeSantis TZ, Hugenholtz P, Larsen N, *et al.* Greengenes, a chimera-checked 16S rRNA gene database and workbench compatible with ARB. *Appl Environ Microbiol* 2006;**72**:5069–72. doi:10.1128/AEM.03006-05
- 10 Ritari J, Salojärvi J, Lahti L, *et al.* Improved taxonomic assignment of human intestinal 16S rRNA sequences by a dedicated reference database. *BMC Genomics* 2015;**16**:1056. doi:10.1186/s12864-015-2265-y
- 11 Caporaso JG, Bittinger K, Bushman FD, *et al.* PyNAST: a flexible tool for aligning sequences to a template alignment. *Bioinforma Oxf Engl* 2010;**26**:266–7. doi:10.1093/bioinformatics/btp636
- 12 Price MN, Dehal PS, Arkin AP. FastTree: computing large minimum evolution trees with profiles instead of a distance matrix. *Mol Biol Evol* 2009;**26**:1641–50. doi:10.1093/molbev/msp077
- 13 Lozupone C, Knight R. UniFrac: a New Phylogenetic Method for Comparing Microbial Communities. *Appl Environ Microbiol* 2005;**71**:8228–35. doi:10.1128/AEM.71.12.8228-8235.2005

Supplementary tables

Series	Age	Total CFU	Bacterial species 1 (% total)	Bacterial species 2 (% total)	Bacterial species 3 (% total)	Bacterial species 4 (% total)	Bacterial species 5 (% total)
1	6w	0	-				
	6w	22	<i>Lactobacillus murinus</i> (40%)	<i>Lactobacillus reuteri</i> (40%)	<i>Lactobacillus intestinalis</i> (10%)	<i>Parabacteroides goldsteinii</i> (10%)	
	11w	13	<i>L. murinus</i> (24%)	<i>L. reuteri</i> (24%)	<i>L. intestinalis</i> (24%)	<i>Lactobacillus johnsonii</i> (24%)	<i>Escherichia coli</i> (4%)
	11w	0	-				
	17w	4	<i>L. murinus</i> (50%)	<i>L. johnsonii</i> (50%)			
	17w	31	<i>L. murinus</i> (34%)	<i>E. coli</i> (33%)	<i>Enterococcus gallinarum</i> (33%)		
	Diabetic	50	ND				
	Diabetic	52	<i>L. murinus</i> (60%)	<i>L. reuteri</i> (35%)	<i>Parabacteroides distasonis</i> (5%)		
	B6	2	<i>E. coli</i> (50%)	<i>Enterococcus gallinarum</i> (50%)			
2	6w	5	<i>L. murinus</i> (100%)				
	6w	0	-				
	6w	0	-				
	11w	0	-				
	11w	15	<i>L. murinus</i> (100%)				
	11w	22	<i>L. murinus</i> (80%)	<i>E. coli</i> (20%)			
	17w	9	<i>L. murinus</i> (100%)				
	17w	78	<i>L. murinus</i> (95%)	<i>L. reuteri</i> (5%)			
	17w	2	<i>L. intestinalis</i> (50%)	<i>Bacillus licheniformis</i> (50%)			
	Diabetic	11	ND				
	Diabetic	30	<i>L. murinus</i> (70%)	<i>E. coli</i> (30%)			
	Diabetic	28	<i>L. murinus</i> (95%)	<i>L. johnsonii</i> (5%)			

Table S1. Bacteria analysis from the liver of NOD mice. Liver cells from NOD mice at different ages and C57BL/6J control mice (B6) were lysed and then plated on terrific broth agar plates at 37°C in aerobic or anaerobic conditions to evaluate bacterial dissemination (n=2-5 mice per group). Number of CFU and species determination were assessed after 24h (aerobic) or 48h (anaerobic) of culture.

Gene	Forward Primer	Reverse Primer
<i>Gapdh</i>	5'-AACGACCCCTTCATTGAC-3'	5'-TCCACGACATACTCAGCAC-3'
<i>Hprt</i>	5'-AAGCTTGCTGGTGAAAAGGA-3'	5'-TTGCGCTCATCTTAGGCTTT-3'
<i>Il22</i>	5'-CAACTTCCAGCAGCCATACA-3'	5'-GTTGAGCACCTGCTTCATCA-3'
<i>Il17</i>	5'-GCTCCAGAAGGCCCTCAGA-3'	5'-AGCTTTCCTCCGCATTGA-3'
<i>Il23a (p19)</i>	5'-ATAATGTGCCCCGTATCCAG-3'	5'-CTGGAGGAGTTGGCTGAGTC-3'
<i>Ifnγ</i>	5'-ACTGGCAAAAGGATGGTGAC-3'	5'-TGAGCTCATTTGAATGCTTGG-3'
<i>Tnfa</i>	5'-ATAATGTGCCCCGTATCCAG-3'	5'-CTGGAGGAGTTGGCTGAGTC-3'
<i>Gzmb</i>	5'-GGACTGCAAAGACTGGCTTC-3'	5'-ATAACATTCTCGGGGCACTG-3'
<i>Foxp3</i>	5'-CCCAGGAAAGACAGCAACCTT-3'	5'-CCTTGCCTTTCTCATCCAGGA-3'
<i>Fut2</i>	5'-AGTCTTCGTGGTTACAAGCAAC-3'	5'-TGGCTAGGTAGATGGTATCACC-3'
<i>Ocln</i>	5'-ATGTCCGGCCGATGCTCTC-3'	5'-TTTGGCTGCTCTTGGGTCTGTAT-3'
<i>Muc2</i>	5'-CCCAGAAGGGACTGTGTATG-3'	5'-TGCAGACACACTGCTCACA-3'
<i>Cldn4</i>	5'-CGCTACTCTTGCCATTACG-3'	5'-ACTCAGCACACCATGACTTG-3'
<i>Tjp1</i>	5'-ACCCGAAACTGATGCTGTGGATAG-3'	5'-AAATGGCCGGGCAGAACTTGTGTA-3'
SFB	5'-GACGCTGAGGCATGAGAGCAT-3'	5'-GACGGCACGGATTGTTATTCA-3'
UTB	5'-ACTCCTACGGGAGGCAGCAG-3'	5'-ATTACCGCGGCTGCTGG-3'
16S rRNA	5'-TGGCTCAGGACGAACGCTGGCGGC-3'	5'-CCTACTGCTGCCTCCCGTAGGAGT-3'

Table S2. Sequences of primers used for RT-qPCR and qPCR.

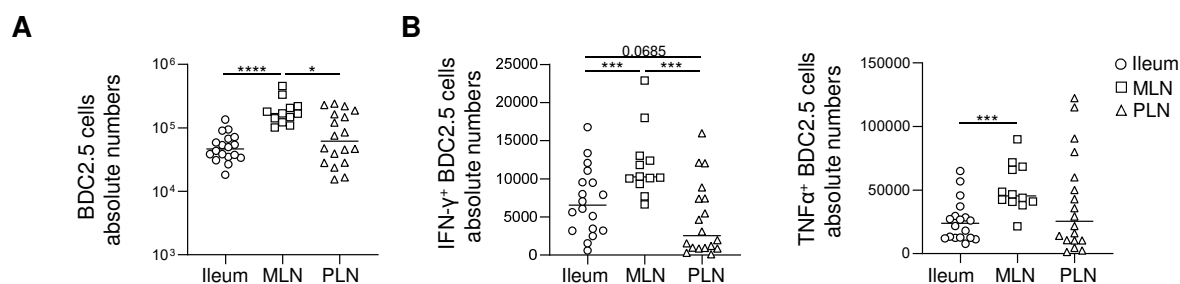


Figure S2. Analysis of transferred BDC2.5 T cells in *Trac*^{-/-} NOD mice.

After *i.v.* injection of CD45.2⁺ CD4⁺ CD62L⁺ T cells from BDC2.5 *Trac*^{-/-} NOD mice into CD45.1⁺ *Trac*^{-/-} NOD mice, ileum, MLN, and PLN from recipient mice were collected and analyzed. **(A)** Absolute cell numbers of CD45.2⁺ TCR β ⁺ BDC2.5 T cell in ileum, MLN, and PLN of *Trac*^{-/-} NOD recipient mice at day 13 after BDC2.5 T cell transfer (n=12-18 per group), corresponding to Figure 5H. **(B)** Absolute cell numbers of IFN- γ ⁺ and TNF α ⁺ BDC2.5 T cells stimulated by PMA/ionomycin in ileum, MLN, and PLN on day 13 after BDC2.5 T cell transfer into *Trac*^{-/-} NOD recipient mice (n=12-18 per group), corresponding to Figure 5J. Horizontal lines indicate the median, each data point represents two pooled mice. *P<0.05, **P<0.01, ***P<0.001 and ****P<0.0001 (two-tailed Mann-Whitney test).

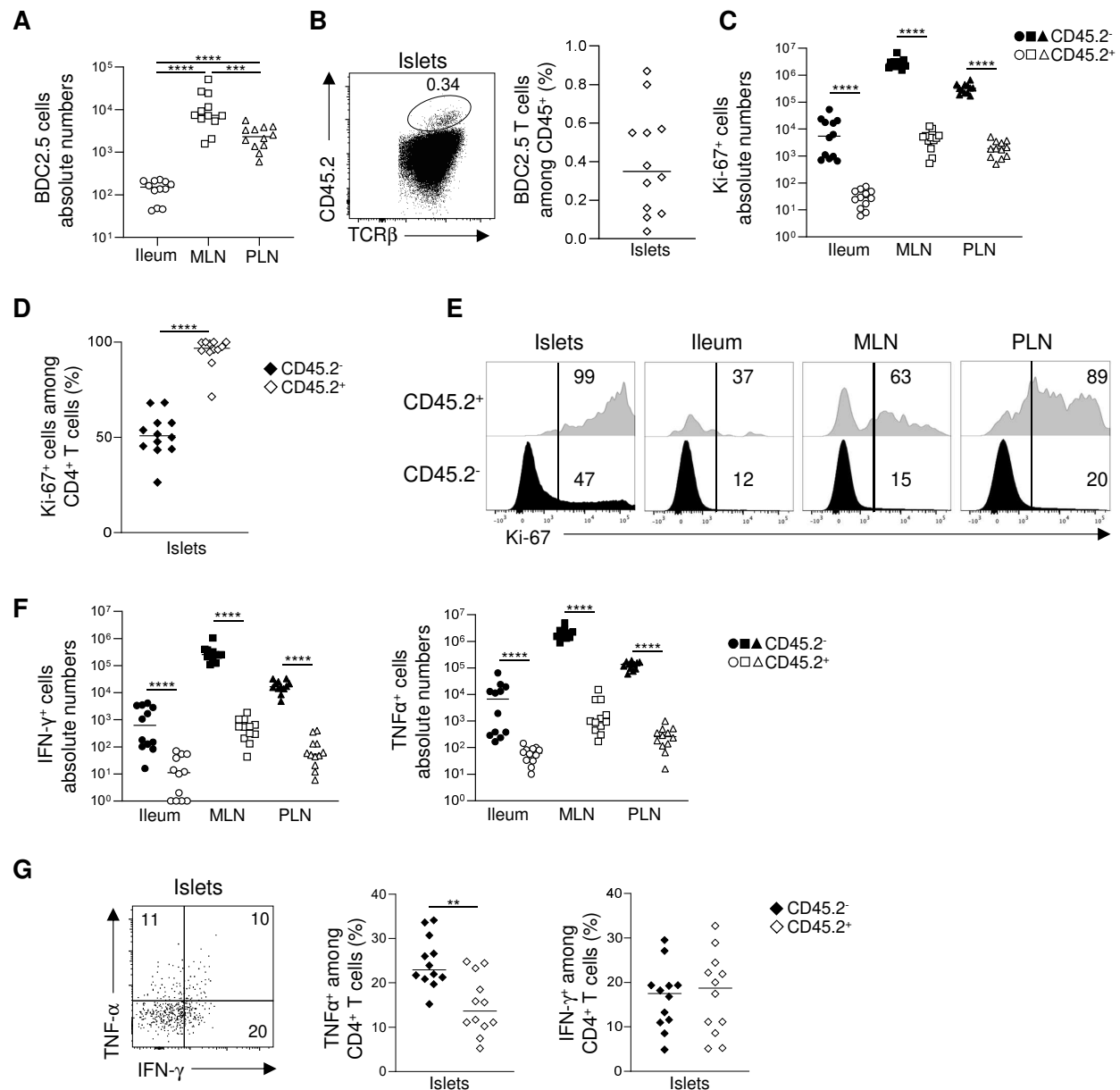


Figure S3. Analysis of transferred BDC2.5 T cells in NOD mice.

After *i.v.* injection of CD45.2⁺ CD4⁺ CD62L⁺ T cells from BDC2.5 *Trac*^{-/-} NOD mice into CD45.1⁺ NOD mice, islets, ileum, MLN, and PLN from recipient mice were collected at day 8 and analyzed. (A) Absolute cell numbers of CD45.2⁺ TCR β ⁺ BDC2.5 T cells (n=12 per group), corresponding to Figure 5L. (B) Representative dot-plot and frequency of BDC2.5 transferred cells in NOD mice islets (n=12). (C) Absolute cell numbers of Ki-67⁺ cells in CD45.2⁺ or CD45.2⁻ cells in ileum, MLN, and PLN (n=12 per group), corresponding to Figure 5M. (D) Frequency of Ki-67⁺ cells in CD45.2⁺ or CD45.2⁻ cells among CD4⁺ T cells in islets (n=12 per group). (E) Histogram representative of Ki-67 staining in CD45.2⁺ (gray) or CD45.2⁻ (black) cells among CD4⁺ T cells in islets, ileum, MLN, and PLN. (F) Absolute cell numbers of IFN- γ ⁺ and TNF α ⁺ cells in CD45.2⁺ BDC2.5 or CD45.2⁻ cells in ileum, MLN, and PLN (n=12 per group), corresponding to Figure 5O. (G) Representative dot-plot and frequencies of TNF α or IFN- γ cytokine expression in CD45.2⁺ or CD45.2⁻ cells among CD4⁺ T cells in islets (n=12 per group). Horizontal lines indicate the median, each data point represents two pooled mice. **P*<0.05, ***P*<0.01, ****P*<0.001 and *****P*<0.0001 (two-tailed Mann-Whitney test).

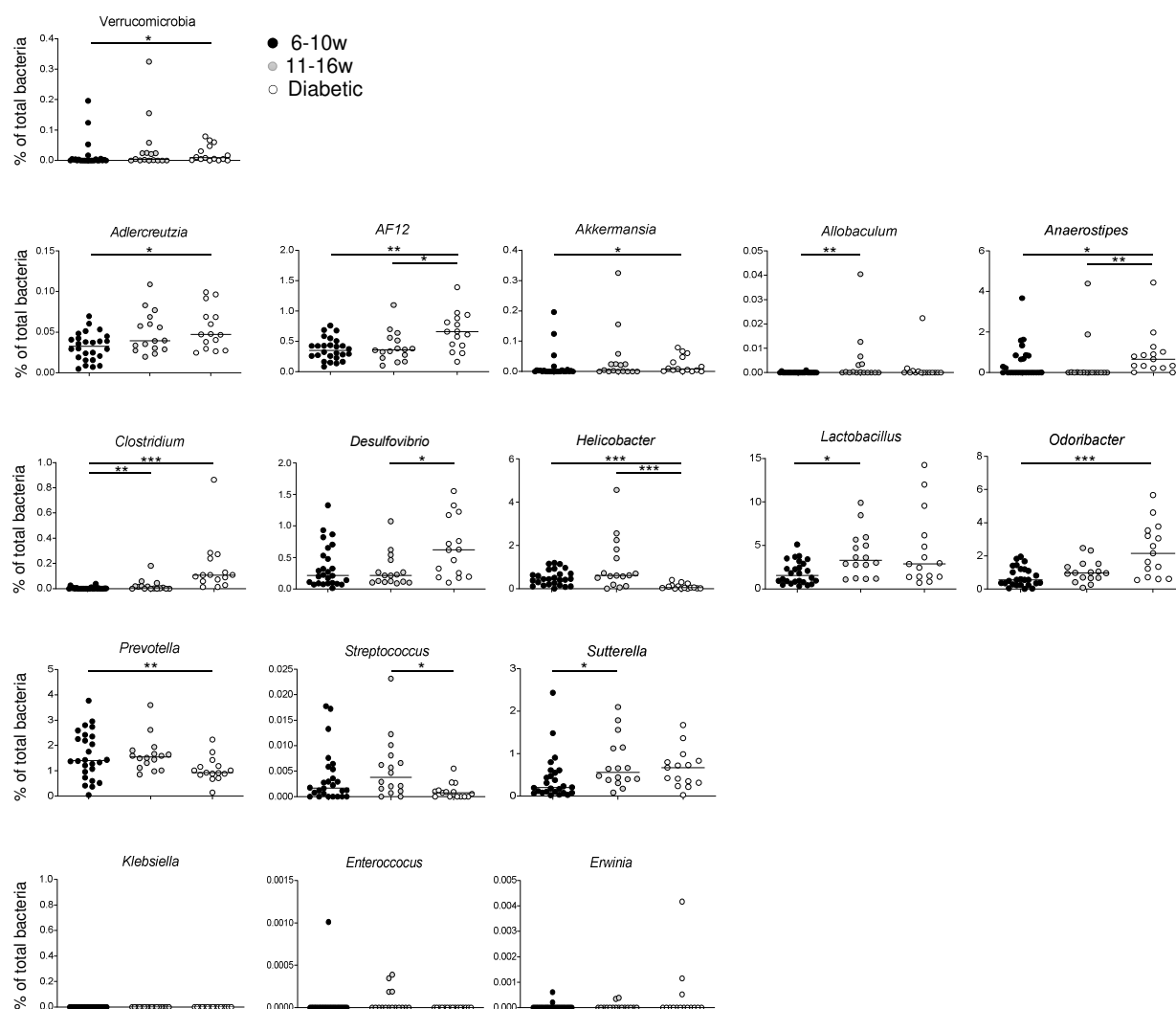


Figure S4. 16S Sequencing plots of bacterial phyla and genera during NOD mice disease progression. Microbiota composition was determined by 16S bacterial DNA sequencing of feces from NOD mice as described in figures 2 and 6. Detailed analysis of the bacterial phyla and genera during T1D development in NOD mice (n=14-26 mice per group). Horizontal lines indicate the median, each data point represents one individual. *P<0.05 (Kruskal–Wallis test with Dunn's Multiple Comparison post-test).

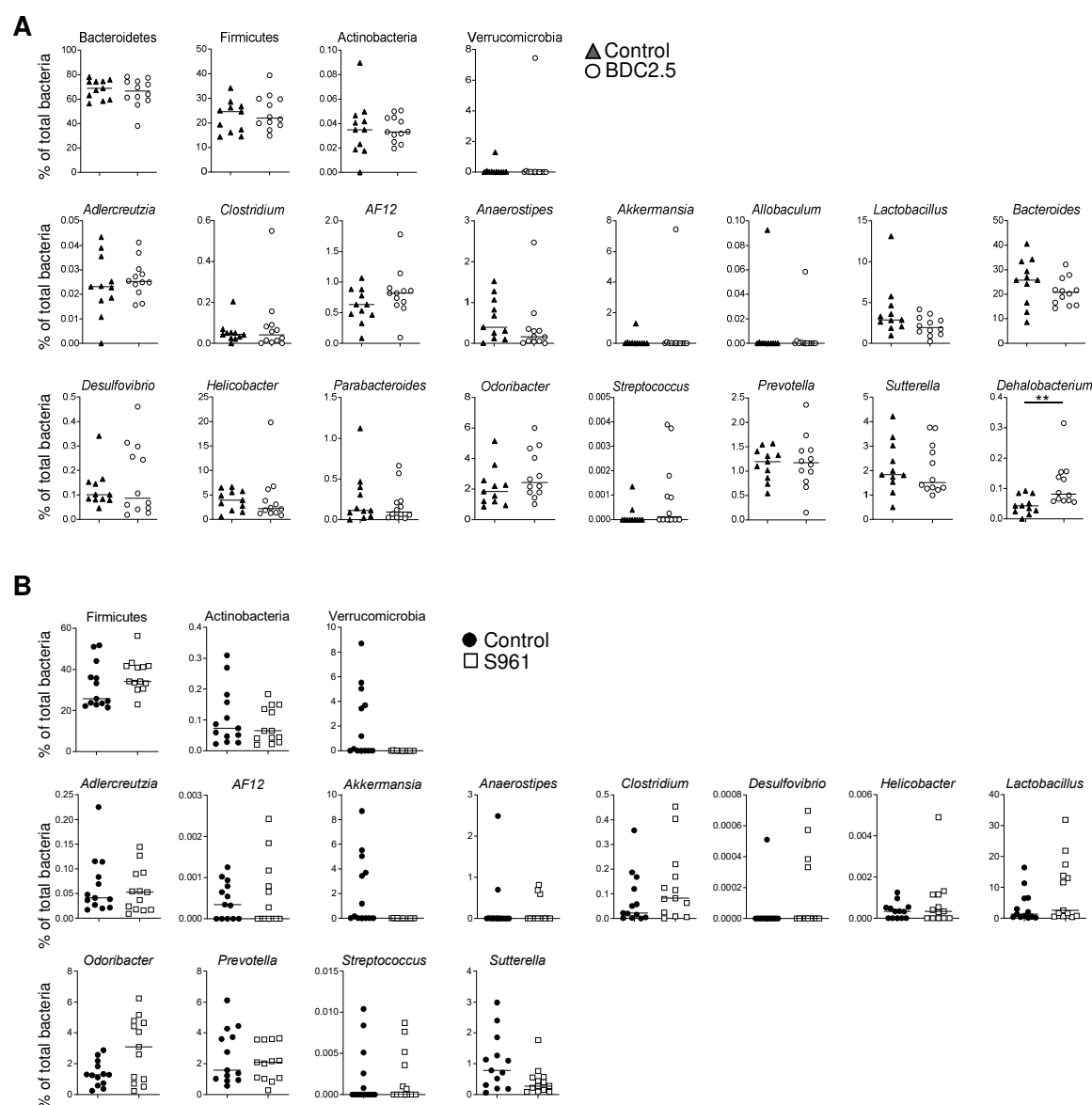


Figure S5. 16S Sequencing plots of bacterial phyla and genera in *Trac*^{-/-} NOD recipient mice transferred with BDC2.5 T cells and in S961-treated mice. Microbiota composition was determined by 16S bacterial DNA sequencing of feces of recipient *Trac*^{-/-} NOD mice transferred with BDC2.5 T cells and from C57BL/6J mice grafted with S961-containing pumps, as respectively described in figures 4-6. **(A)** Detailed analysis of the phyla and genera in recipient mice after BDC2.5 T cell transfer or not in *Trac*^{-/-} NOD mice (n=11-13 mice per group). **(B)** Detailed analysis of the phyla and genera after hyperglycemia induction or not in C57BL/6J mice (n=13 mice per group). Horizontal lines indicate the median, each data point represents one individual. *P<0.05, **P<0.01 (two-tailed Mann-Whitney test).

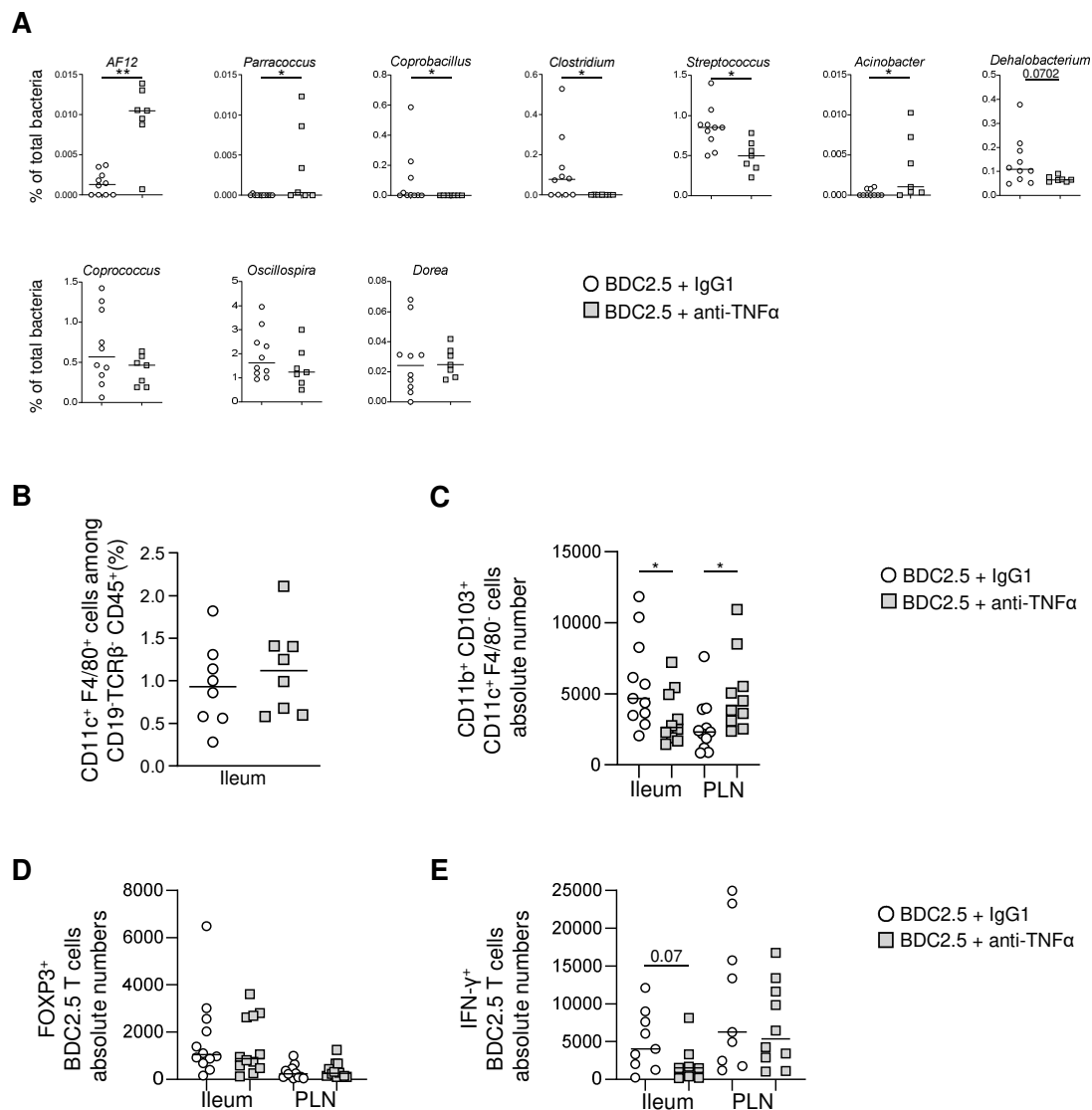


Figure S6. Analysis of bacterial phyla, genera and immune cells in *Trac*^{-/-} NOD mice transferred with BDC2.5 T cells and receiving anti-TNFα treatment. (A) Microbiota composition was determined by 16S bacterial DNA sequencing of feces of recipient *Trac*^{-/-} NOD mice transferred with BDC2.5 T cells and treated with anti-TNFα or human control IgG1 antibodies as described in figure 7. Detailed analysis of bacterial genera in recipient mice after BDC2.5 T cell transfer and anti-TNFα or human control IgG1 antibodies treatment (n=7-10 per group). (B) CD11c⁺ F4/80⁺ macrophages frequency in BDC2.5 transferred *Trac*^{-/-} mice ileum were analyzed by flow cytometry with IgG1 or anti-TNFα treatment (n=8 per group). (C) Absolute cell numbers of CD11c⁺ CD11b⁺ CD103⁺ F4/80⁺ DCs in ileum and PLN from *Trac*^{-/-} NOD recipient mice treated with anti-TNFα or control IgG1 antibodies (n=10-11 per group), corresponding to Figure 7F. (D-E) Absolute cell numbers of FOXP3⁺ cells in BDC2.5 T cells (D) and IFN-γ cytokine expression in PMA ionomycin activated BDC2.5 T cells (E) in ileum and PLN on day 13; after BDC2.5 T cell transfer into *Trac*^{-/-} NOD recipient mice treated with anti-TNFα or control IgG1 antibodies (n=8-12 per group), corresponding to Figure 7H and Figure 7I. Horizontal lines indicate the median, each data point represents one individual. *P<0.05 and **P<0.01 (two-tailed Mann-Whitney test).

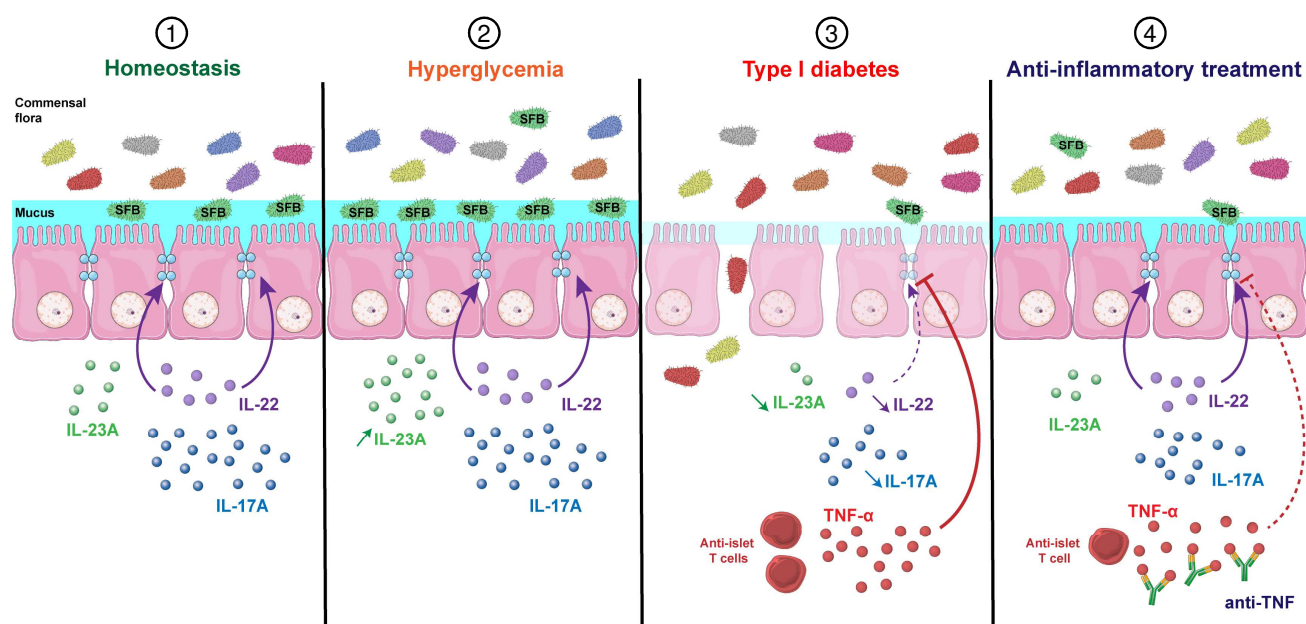


Figure S7. Graphical abstract of gut mucosa alteration and SFB loss induced by inflammation in T1D rather than hyperglycemia and recovered by anti-TNF α treatment.

(1) As already known, intestinal IL-17A and IL-22 participate in the maintenance of gut integrity and both can be induced by Segmented Filamentous Bacteria (SFB). (2) Hyperglycemia with no inflammation did not reduced SFB abundance, the level of IL-17A, IL-22 and IL-23A and epithelial function in the ileum. (3) Mouse models of auto-immune T1D exhibit gut microbiota and mucosa alterations. In addition to loss of IL-17A, IL-22, and IL-23A in gut mucosa, gut integrity is impaired and associated with dysbiosis including progressive loss of SFB. (4) Anti-inflammatory treatment restores gut mucosa homeostasis and intestinal immune cell function and SFB abundance.